CELL BIOLOGY

A Rhesus channel in the coral symbiosome membrane suggests a novel mechanism to regulate NH_3 and CO_2 delivery to algal symbionts

Angus B. Thies[1]*, Alex R. Quijada-Rodriguez[2], Haonan Zhouyao[2], Dirk Weihrauch[2], Martin Tresguerres[1]*

Reef-building corals maintain an intracellular photosymbiotic association with dinoflagellate algae. As the algae are hosted inside the symbiosome, all metabolic exchanges must take place across the symbiosome membrane. Using functional studies in *Xenopus* oocytes, immunolocalization, and confocal Airyscan microscopy, we established that *Acropora yongei* Rh (ayRhp1) facilitates transmembrane NH_3 and CO_2 diffusion and that it is present in the symbiosome membrane. Furthermore, ayRhp1 abundance in the symbiosome membrane was highest around midday and lowest around midnight. We conclude that ayRhp1 mediates a symbiosomal NH_4^+-trapping mechanism that promotes nitrogen delivery to algae during the day—necessary to sustain photosynthesis—and restricts nitrogen delivery at night—to keep algae under nitrogen limitation. The role of ayRhp1-facilitated CO_2 diffusion is less clear, but it may have implications for metabolic dysregulation between symbiotic partners and bleaching. This previously unknown mechanism expands our understanding of symbioses at the immediate animal-microbe interface, the symbiosome.

INTRODUCTION

Photosymbiotic associations between invertebrates and microalgae are widespread in aquatic environments. Perhaps the most well known of these partnerships is that of reef-building corals (phylum: Cnidaria) and dinoflagellate symbiotic algae (family: Symbiodiniaceae), which is key to the evolutionary success of coral reef ecosystems (*1*). In an otherwise oligotrophic environment, the cnidarian host satisfies the majority of its energetic needs using photosynthates derived from its symbiotic algae (*2*). The host cells are believed to exercise considerable control over the metabolism of their symbionts, which favors both the production and release of algal photosynthates. This control is possible because of an architectural arrangement whereby coral gastrodermal cells host the algal symbionts intracellularly within an arrested phagosome known as the symbiosome [reviewed in (*3*)]. Because the symbiosome isolates the alga from the cytosol of the host cell, the symbiosome membrane necessarily mediates all metabolic exchanges between the symbiotic partners. In addition, the symbiosome membrane may serve as an interface for the coral to manipulate the alga's microenvironment. For example, the coral symbiosome is markedly acidic (pH ~4) because of active H^+ pumping by V-type H^+-ATPases (VHAs) located in the symbiosome membrane (*4*). The acidic nature of the symbiosome drives CO_2 accumulation as part of a carbon concentrating mechanism (CCM) that helps overcome the low affinity of algal Rubisco for CO_2, thereby promoting algal photosynthesis (*4*). This H^+ gradient has been proposed to additionally energize the movement of other essential nutrients and metabolites into or out of the symbiosome including nitrogen, phosphorus, and sugars (*3*, *4*). However, no additional molecular players or regulatory mechanisms have been definitely identified to date.

The vast majority of the symbiotic algae's nitrogen demand is supplied by protein catabolism by their animal host, which produces waste as ammonia gas (NH_3) and ammonium ion (NH_4^+), which exist in a pH-dependent equilibrium [collectively referred to as "total ammonia" (Tamm)] (*2*, *5*). Rather than excreting its nitrogenous waste into the environment like most other aquatic animals (*6*), the coral symbiosis recycles a substantial portion of Tamm via the glutamine synthase/glutamate dehydrogenase/glutamine oxoglutarate aminotransferase pathways (GS/GDH/GOGAT) (*5*, *7*, *8*). In addition, corals are able to take up NH_4^+ from seawater and transport it to their algal symbionts (*9*), and isolated algal symbionts take up and use NH_4^+ (*10*). Moreover, coral host cells are known to regulate Tamm delivery to their symbionts, and as a result, the algae accumulate significantly more nitrogen in the light than in the dark (*9*, *11*). The diel regulation of Tamm delivery by corals allows for host control over the carbon and nitrogen metabolisms of symbionts (*12*) and, by extension, the growth rate and biomass of the symbiont population to prevent symbiont overgrowth that would disrupt the symbiosis (*13*). Transcriptomic analyses on whole coral colonies have identified candidate transporters proposed to mediate Tamm delivery to symbionts (*14*), but a lack of localization studies precludes a definite assessment of their involvement in symbiosis. Overall, the mechanisms that mediate and regulate nitrogen transport to symbionts across the symbiosome membrane remain unknown.

NH_3 and NH_4^+ exist in pH-dependent equilibrium with pKa ~9.25, and thus >96% of Tamm is found as NH_4^+ both in seawater (pH ~8) and in coral host cells (pH ~7.4) (*15*). However, the much lower pH in the symbiosome space has three critical and interlinked implications: first, a virtually nil NH_3 partial pressure (pNH_3) in the symbiosome space that should drive NH_3 gas diffusion from the host cytoplasm; second, the immediate "trapping" of NH_3 as NH_4^+ in the symbiosome space, which can be taken up by the alga, thus maintaining the inwardly directed NH_3 diffusion gradient; and lastly, an unfavorable electrochemical gradient for NH_4^+ transport into the symbiosome.

However, despite being a gas, NH_3 has limited permeability through lipidic membranes because of its strong dipole moment that makes

[1]Marine Biology research Division, Scripps Institution of Oceanography, University of California, San Diego, La Jolla, CA 92093, USA. [2]Department of Biological Sciences, University of Manitoba, Winnipeg, MB, Canada.
*Corresponding author. Email: athies@ucsd.edu (A.B.T.); mtresguerres@ucsd.edu (M.T.)

it a polar molecule [reviewed in (*16*)]. In some plant-bacteria symbioses, NH_3 transport across the symbiosome membrane is facilitated by nodulin-intrinsic proteins (*17*, *18*); however, this protein family is exclusive to plants. In addition, NH_3 diffusion across biological membranes can be significantly enhanced by Rhesus (Rh) channels, a family of evolutionary conserved proteins present in eubacterial, invertebrate, and vertebrate lineages (*19*–*21*). On the basis of the observed up-regulation of an Rh-like mRNA transcript upon establishment of symbiosis in anemones (*22*–*24*), Rh channels have been suggested to play important roles in cnidarian-algae symbioses. However, the Rh-like mRNA was expressed in many soft coral cell subtypes (*25*), and therefore, the coded protein probably plays multiple physiological roles. In addition, Rh channels are typically present in the cell outer plasma membrane [reviewed in (*16*, *26*)], and few studies have localized Rh-like proteins to intracellular compartments or organelles (*27*, *28*). Last, the various Rh protein isoforms have different substrate specificity: some may transport both NH_3 and NH_4^+ (*16*), some act as dual NH_3 and CO_2 gas channels (*19*, *29*, *30*), and others do not facilitate Tamm/CO_2 transport across membranes at all and have structural functions instead (*31*, *32*). However, detailed functional studies about transport properties by "primitive" Rh proteins from invertebrate animals (termed "Rhp") are very scarce. As a result, assessing the physiological role of the coral Rh-like coded protein and its potential involvement in delivering Tamm to algal endosymbionts requires elucidating its actual function as well as its cellular and subcellular localizations. Furthermore, if coral Rh facilitated CO_2 diffusion and was present on the symbiosome membrane, it would provide a pathway for CO_2 backflow from the symbiosome into the coral gastrodermal cells and affect interactions between nitrogen transport and the CCM.

Given that NH_3 diffusion through biological membranes is limited, we hypothesized that corals use Rh-like proteins to deliver NH_3 to their algae across the symbiosome membrane, which would subsequently get trapped as NH_4^+ in the acidic symbiosome. To investigate this possibility, we cloned an Rh-like gene from the coral *Acropora yongei* (*ayRhp1*) and determined its phylogenetic relationship to other Tamm-transporting proteins. Then, we heterologously expressed ayRhp1 protein in *Xenopus* oocytes and measured Tamm transport under a range of pHs to determine whether it transports NH_3, NH_4^+, or both. In additional oocyte experiments, we determined whether ayRhp1 facilitates CO_2 diffusion. Using custom-made antibodies and immunocytochemistry, we established the localization of ayRhp1 protein in the various cell subtypes throughout the coral colony, and, using confocal Airyscan microscopy, we investigated whether ayRhp1 was specifically located in the symbiosome membrane. Last, we quantified the subcellular localization of ayRhp1 within algae-containing coral gastrodermal cells throughout a diel cycle to explore a potential mechanism whereby coral host cells could regulate Tamm delivery to their algal symbionts.

RESULTS AND DISCUSSION

Rhp1 genes are widespread in corals

The cloned *ayRhp1* cDNA open reading frame contains 1440 base pairs encoding a protein with a predicted molecular weight of 51.8 kDa. BLAST searches in genomic and transcriptomic databases revealed predicted ayRhp1 homologs in multiple coral species from both the robust and complex clades, which diverged from each other 300 million to 400 million years ago (*33*). These coral Rh proteins clustered together with *Rhp1* genes from invertebrate animals (fig. S1).

The protein features of ayRhp1 are similar to those of well-studied Rh channels from mammals (fig. S2). It has 12 transmembrane helices and an N-linked glycosylation site (N61), which differentiate all animal Rh50 channels capable of Tamm transport (Rhag-cg, Rhp1-2) (*16*) from the Rh30 proteins involved in structural functions (*27*). Crystallography and simulation studies have identified several key amino acid residues that are required for NH_3 transport across mammalian RhCG (*20*, *21*): a phenylalanine gate (F130 and F235) and a cytosolic shunt (L193, T325, L328, I334, N341, and N342), which recruit NH_4^+ at the external and internal vestibules, respectively, twin histidines that deprotonate NH_4^+ to NH_3 (H185 and H344), two highly conserved aspartic acid residues that help shuttle the H^+ back to the original compartment (D177 and D336), and a hydrophobic transmembrane channel that selectively conducts NH_3 but not NH_4^+ (*32*, *34*). An alignment of ayRhp1 with RhCG reveals that the phenylalanine gate (F147 and F251), the twin histidines (H202 and H364), and analogous aspartate residues (D195 and D356) are all conserved in ayRhp1, while the cytosolic shunt and hydrophobic channel-lining residues are highly conserved (~83 and ~70%, respectively). In addition, ayRhp1 contains the nine residues that form the putative cytoplasmic CO_2 binding pocket of mammalian RhCG [which facilitates CO_2 transport (*19*)]: L91, F94, D234, A237, M238, M299, V300, Q303, and N304. Six of these residues are also conserved in the Rh protein from the bacterium *Nitrosomonas europaea*, where the CO_2 binding pocket was definitely identified using x-ray crystallography (*35*). In summary, the overall high conservation of these key structures suggests that ayRhp1 can facilitate both NH_3 and CO_2 transport; this was experimentally tested through functional studies.

ayRhp1 facilitates NH_3 and CO_2 diffusion

ayRhp1 was functionally characterized by measuring Tamm uptake rates in *Xenopus* oocytes injected with ayRhp1 cRNA. To avoid potential artifacts resulting from using radiolabeled [^{14}C]-methylammonium as a Tamm analog (*16*), we used a hypochlorite-salicylate-nitroprusside–based colorimetric assay to directly measure Tamm accumulation in oocytes and estimate Tamm uptake rate. The bath solutions contained 1 mM Tamm at pH 6.5, 7.5, or 8.5, resulting in 10-fold pKa-dependent [NH_3] increases for every pH unit (1.8, 17.4, and 150.5 μM, respectively). ayRhp1-expressing oocytes had consistently higher Tamm uptake rates than those of controls in all conditions tested ($P < 0.001$; fig. S3). In addition, Tamm uptake rate in ayRhp1 oocytes significantly increased from 10.2 ± 1.4 pmol Tamm min^{-1} at pH 6.5, to 36.9 ± 2.8 pmol Tamm min^{-1} at pH 7.5, and to 49.6 pmol Tamm min^{-1} at pH 8.5 (Fig. 1A), an apparent J_{max} and K_m of 51.93 ± 1.45 pmol Tamm min^{-1} and 7.14 ± 0.91 μmol Tamm liter^{-1}, respectively (Fig. 1B). These results indicate that ayRhp1 transports NH_3 following the partial pressure difference. In addition, Tamm uptake rate of oocytes incubated in a solution with 10 mM Tamm at pH 7.5 was 50.3 ± 10.0 pmol Tamm min^{-1} (i.e., indistinguishable from the rate in the 1 mM Tamm pH 8.5 solution) (Fig. 1B). These two solutions have similar [NH_3] (174.0 versus 150.5 μM), but the former has >10-fold greater [NH_4^+] than the latter (9826.0 μM versus 849.5 μM). Together, these results established that ayRhp1 can facilitate NH_3 diffusion following pH-dependent partial pressure gradients and that Tamm transport is not directly dependent on the [NH_4^+] difference.

Next, we preloaded control and ayRhp1 cRNA-injected oocytes with 5% CO_2 and measured CO_2 release into normocapnic media

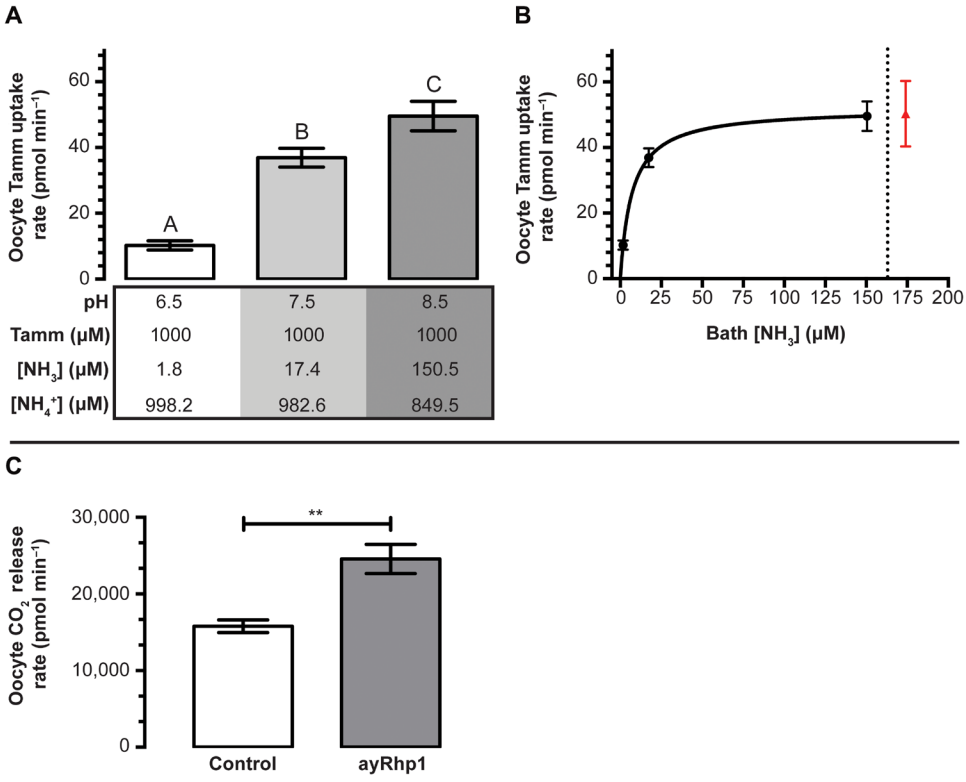

Fig. 1. Functional characterization of total ammonia (Tamm) and CO_2 transport by *Acropora yongei* Rhesus protein (ayRhp1). (**A**) Effect of [NH_3] on Tamm uptake rate in *Xenopus* oocytes expressing ayRhp1. Control Tamm uptake rates have been subtracted. Data show means ± SEM of six to eight oocytes; the letters denote significant differences [one-way analysis of variance (ANOVA) followed by Tukey's multiple comparisons test; pH 6.5 versus pH 7.5, $P < 0.0001$; pH 7.5 versus pH 8.5, $P = 0.0222$; pH 6.5 versus pH 8.5, $P < 0.0001$]. (**B**) Michaelis-Menten Tamm uptake kinetics calculated from the data shown in (A) (black dots to the left of the dotted line). Apparent $J_{max} = 51.93 \pm 1.45$ pmol Tamm min^{-1} and $K_m = 7.14 \pm 0.91$ μmol Tamm $liter^{-1}$. The red triangle indicates Tamm uptake rate obtained in a solution with 10 mM Tamm at pH 7.5 (175 μM NH_3 and 9.825 mM NH_4^+) (i.e., similar [NH_3] to the previous data point, but ~10-fold higher [NH_4^+]). (**C**) Functional characterization of CO_2 transport by ayRhp1. *Xenopus* oocytes expressing ayRhp1 (ayRhp1) display a higher rate of CO_2 release than control oocytes after equal CO_2 preloading. Data show means ± SEM of $n = 8$, 25 oocytes per n; ** denotes significant differences (Welch's t test; $P = 0.0019$).

using a custom-built CO_2 analyzer (*36*). These experiments revealed that ayRhp1-expressing oocytes released CO_2 at a rate ~50% faster than control oocytes ($P = 0.0019$; Fig. 1C). As wild-type *Xenopus* oocytes lack notable HCO_3^- efflux (*37*), this demonstrates that ayRhp1 can facilitate the diffusion of CO_2 in addition to NH_3.

ayRhp1 protein is present in multiple coral cell types

Immunofluorescence microscopy using custom-made–specific antibodies revealed high ayRhp1 protein expression throughout *A. yongei* coral tissue sections (Fig. 2A). In the epidermis, ayRhp1 was present in the apical membrane of columnar cells along the seawater-coral interface (Figs. $2B_1$ and 3A). Although corals recycle most of their nitrogen waste through their algal symbionts, they also excrete some Tamm to the environment (*2*, *7*). Thus, we hypothesize that ayRhp1 in epidermal cells aids in nitrogenous waste excretion as previously described in gills and skin from fish and aquatic invertebrates (*38*, *39*). Moreover, Tamm excretion may be facilitated by stirring of the boundary layer by ciliary beating, akin to mussels and polychaetes (*38*, *40*).

In the calicodermis, ayRhp1 was expressed in both calcifying cells that deliver dissolved inorganic carbon (DIC), Ca^{2+}, and matrix proteins for skeletal formation and in desmocytes that anchor living coral tissue to the skeleton. The ayRhp1 signal in desmocytes was very intense, especially at the apical membrane adjacent to the skeleton (Figs. $2C_1$ and 3B and fig. $S4A_1$). Previous studies have provided morphological descriptions of coral desmocytes (*41*, *42*); however, to our knowledge, this is the first description of any protein specifically expressed in this cell type. As an NH_3 channel, ayRhp1 may contribute to coral calcification by enhancing NH_3 diffusion to buffer the pH of the extracellular calcifying medium (ECM) and maintain conditions favorable for calcification. Metabolic NH_3 has been proposed to promote biological calcification of avian egg shells (*43*), land snail shells (*44*), and coral skeletons (*45*) by buffering H^+ produced during $CaCO_3$ precipitation as NH_4^+. As a CO_2 channel, ayRhp1 could help deliver DIC to the ECM following the outwardly directed pCO_2 gradient favoring CO_2 diffusion from calicodermis cells into the ECM, which is an important source of DIC for calcification in multiple coral species (*46*, *47*). In the gastroderm, ayRhp1 was highly expressed in alga-hosting coral cells surrounding the symbiotic algae (Fig. $2D_1$), in a pattern that resembled that of VHA in the symbiosome membrane (*4*). This was explored in further detail.

ayRhp1 is present in the symbiosome membrane

Confocal Airyscan microscopy and coimmunostaining of ayRhp1 and Na^+/K^+-ATPase (NKA) allowed us to definitively establish ayRhp1's subcellular localization within the tightly packaged host cells in coral

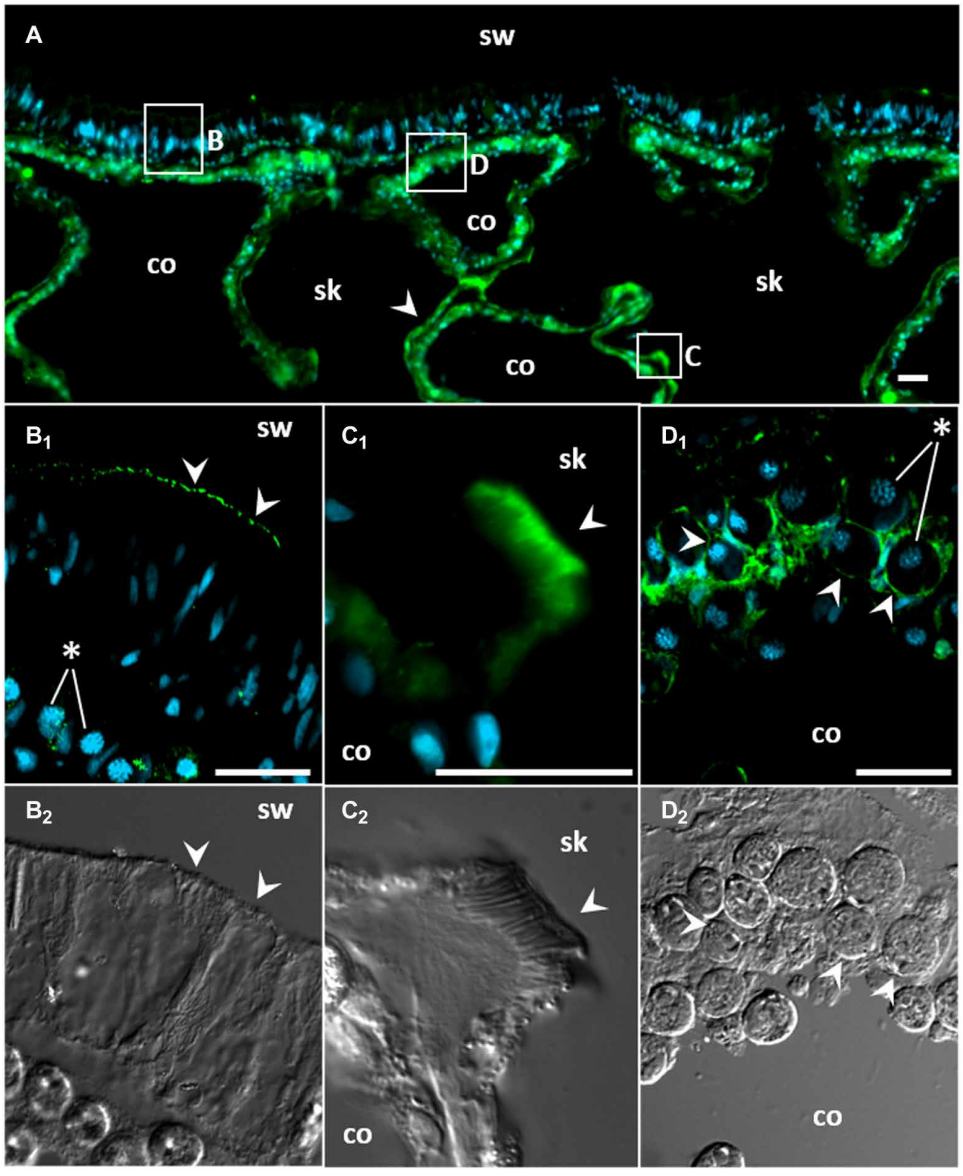

Fig. 2. Immunolocalization of *Acropora yongei* Rhesus protein (ayRhp1). (**A**) Overview of *A. yongei* tissues; the boxes indicate regions of interest shown at higher magnification below, and the white arrowhead indicates ayRhp1-labeled calcifying cells. (**B_1**) Apical membrane of columnar cells in the oral epidermis. (**C_1**) Desmocyte with intense signal in its apical region. (**D_1**) Alga-containing gastrodermal cells. (**B_2**, **C_2**, and **D_2**) Corresponding bright-field differential interference contrast images; the white arrowheads mark corresponding locations in (B), (C), and (D). Coral and algal nuclei are shown in blue, and ayRhp1 immunofluorescence is shown in green. Several algal nuclei are marked with asterisks in (B_1) and (D_1) for clarity. This coral was sampled at midday. sw, seawater; co, coelenteron; sk, skeleton. Scale bars, 20 μm.

tissues. Consistent with its universal presence in the plasma membrane (*48*), NKA outlined the perimeter of all alga-containing host cells (Fig. 4, A and B). The ayRhp1 signal was also present around the algae; but in most cells, it was internal to that of NKA and also present in the thin region between the host cell nucleus and the alga (Fig. 4 A_1). Since these cells are tightly packed, this region is occupied by the symbiosome membrane (*4*, *49*). This was most readily evident in the region adjacent to the coral nucleus where a region of cytosol separates the external NKA and internal ayRhp1 signals, further indicating their respective presence in the plasma and symbiosome membranes (Figs. $4A_2$ and 3). The symbiosomal localization of ayRhp1 was further confirmed in host cells containing two algae (fig. S5C), which are rather scarce but contain a larger cytoplasmic region that allows for better visualization of subcellular compartments. In addition, a minority of cells lacked ayRhp1 in the region between the host nucleus and the algae (Fig. 4B), which instead colocalized with or appeared slightly internal to NKA around the nuclear periphery, indicating ayRhp1's presence in the host plasma membrane, cytosolic vesicles, or both. We attempted to quantify the two ayRhp1 subcellular localization patterns using tissue sections; however, the high density of tightly packed gastrodermal cells coupled with their intense NKA signal confounded imaging and prevented an unbiased approach. To circumvent these limitations, we immunostained isolated coral cells, an approach we previously used to confirm

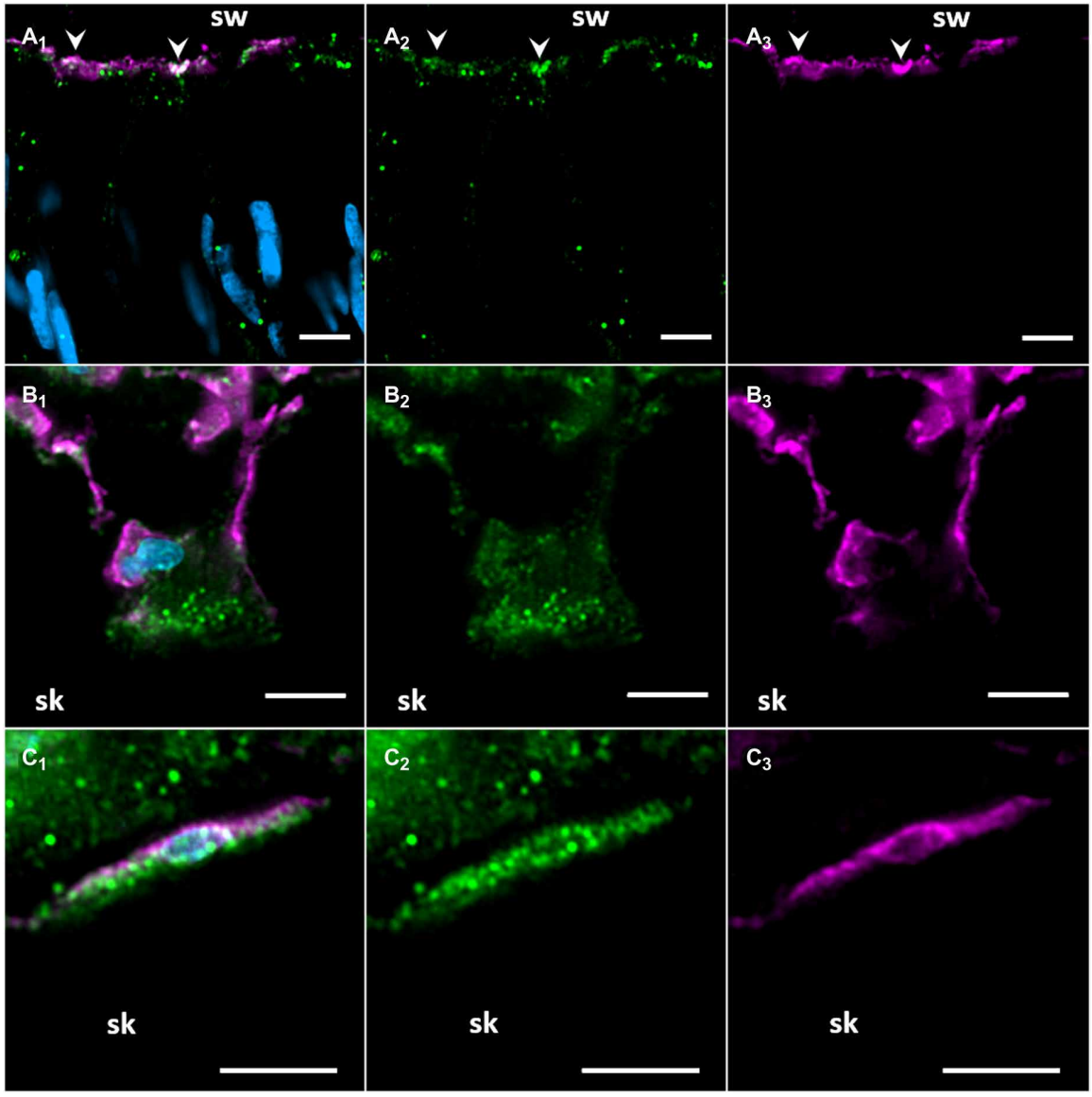

Fig. 3. Confocal Airyscan immunolocalization of *Acropora yongei* Rhesus protein (ayRhp1) in the oral epidermis, desmocytes, and calcifying cells. (**$A_{1–3}$**) ayRhp1 on the apical membrane of columnar cells in the oral epidermis. (**$B_{1–3}$**) Desmocyte with intense ayRhp1 signal in its apical region. (**$C_{1–3}$**) Calcifying cells displaying ayRhp1 signal on membranes and in the cytosol. Corresponding areas between panels are marked with arrowheads. [(A_1) to (C_1)], [(A_2) to (C_2)], and [(A_3) to (C_3)] show ayRhp1, Na^+/K^+-ATPase (NKA), and 4′,6-diamidino-2-phenylindole (DAPI) signals, ayRhp1 signal alone, or NKA signal alone, respectively. Nuclei (DAPI) are shown in blue, ayRhp1 in green, and the NKA in purple. Scale bars, 5 μm.

the presence of VHA in the symbiosome membrane (*4*). Similar to tissue sections, a majority of isolated cells displayed ayRhp1 signal in the thin region between the host cell nucleus and the alga, indicative of ayRhp1 symbiosomal localization (fig. S5, B, C, and E to I). We also observed a minority of cells with ayRhp1 signal around the host cell nucleus (fig. S5, D and J to N), indicative of ayRhp1's presence in the cytoplasm or plasma membrane of the host cell. Free algal cells released during the isolation procedure, identified by the lack of an adjacent host nucleus, did not have ayRhp1 signal (fig. S5A).

Diel trafficking of ayRhp1

On the basis of established patterns of nitrogen delivery to coral algal symbionts (*9*, *11*), we hypothesized that the ayRhp1 subcellular localization would change in a diel fashion. We therefore quantified ayRhp1 subcellular localization patterns using epifluorescence microscopy on isolated alga-containing coral cells over a diel cycle. This allowed us to achieve sufficient replication (50 cells from 18 coral branches, 3 coral branches at each of six time points, for a total of 900 cells observed in blind fashion). Once an algal-containing coral host cell was identified, the observer rapidly and continuously shifted the focal plane and alternated between fluorescence and bright-field DIC while looking through the microscope eyepiece. This technique allowed the observer to determine whether the ayRhp1 signal was present in between the host cell nucleus and the alga (classified as "symbiosomal localization"; Fig. 4A and fig. S5, B, C, and E to I), or around the periphery of the host cell's nucleus ("nonsymbiosomal

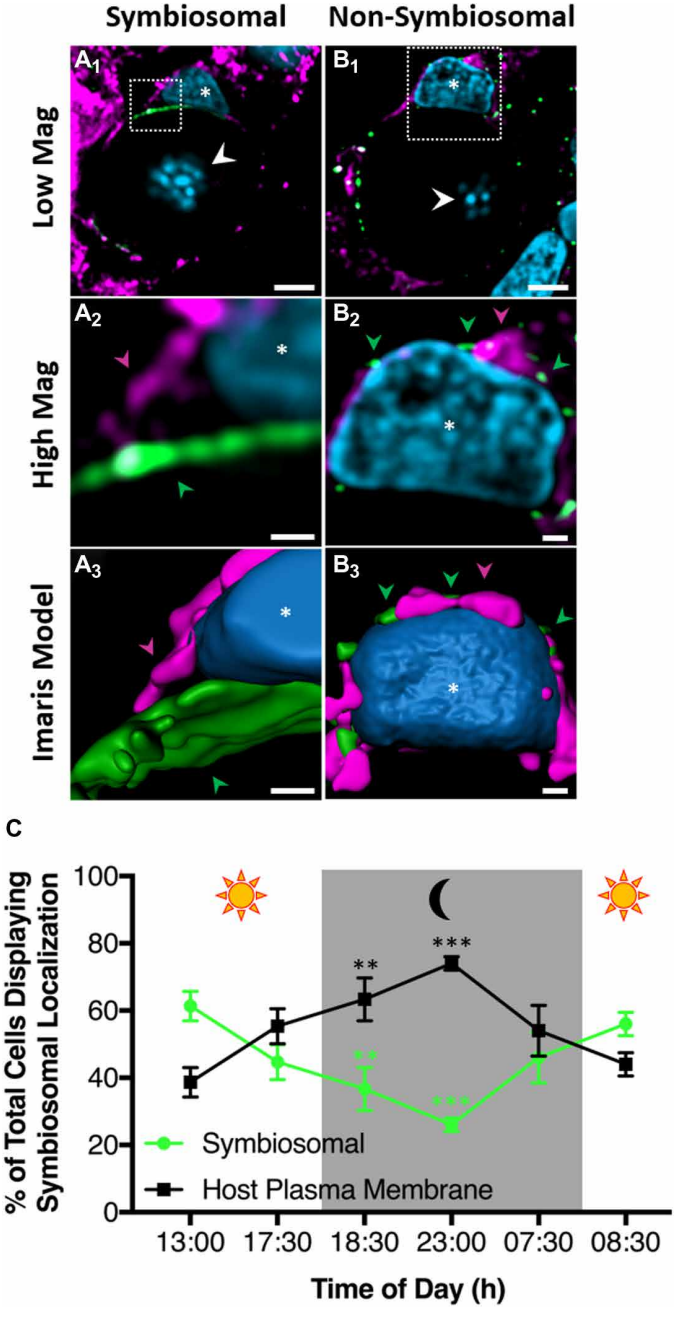

Fig. 4. Confocal Airyscan immunolocalization of *Acropora yongei* Rhesus protein (ayRhp1) in alga-containing coral cells. (**A_1**) Cells displaying ayRhp1 in the symbiosome membrane of tissue sections. (**B_1**) Cells displaying nonsymbiosomal ayRhp1 of tissue sections. (**A_2** and **B_2**) Higher magnification of the region denoted by the white boxes in (A_1) and (B_1). (**A_3** and **B_3**) Three-dimensional renderings of (A_2) and (B_2). Corresponding areas between (A_2) and (B_2) and (A_3) and (B_3) are marked. Nuclei are shown in blue, ayRhp1 in green, and the NKA in purple. Notice the separation ($A_{1–3}$) or colocalization ($B_{1–3}$) of ayRhp1 and NKA corresponding to symbiosomal or nonsymbiosomal ayRhp1 localizations, respectively. Host nuclei are denoted with an asterisk, and algal nuclei with arrowheads. Scale bars, 5 μm (A_1 and B_1), 0.5 μm (A_2 and B_2), and 0.5 μm (A_3 and B_3). (**C**) Percentage of total alga-containing *A. yongei* host cells with symbiosomal ayRhp1 over a diel cycle. Data show means ± SEM. $n = 3$ per time point, 50 cells per n, 900 cells total. The asterisks indicate significant differences with the 1300-hour time point (two-way repeated-measures ANOVA followed by Dunnett's posttest; $^{**}P < 0.01$; $^{***}P < 0.0001$).

localization"; Fig. 4B and fig. S5, D and J to N). The percentage of cells displaying ayRhp1 symbiosomal localization was significantly higher during the day, with a maximum of 61.3 ± 4.4% cells displaying this pattern at 1300 hours in contrast to only 26.0 ± 2.0% of cells at 2300 hours ($P < 0.001$) (Fig. 4C). These results indicate that ayRhp1 is preferentially present in the symbiosome membrane during the day. To our knowledge, this is the first report of diel changes in proteomic makeup of the cnidarian symbiosome membrane and furthers the notion that this interface that separates symbiotic partners can be dynamically modified by the host cell to control the physiology of the alga.

A putative host-controlled nitrogen concentrating mechanism

The pKa for Tamm combined with the pH difference between the host cell's cytosol and the symbiosome dictates >2000 higher pNH_3 in the former. Although this establishes a steep partial pressure gradient favoring NH_3 diffusion into the symbiosome, diffusion across lipidic membranes is generally limited [reviewed in (*16*)]. The presence of ayRhp1 in the symbiosome membrane is poised to overcome this limitation, thus enhancing NH_3 delivery to the algal symbionts in an analogous manner to nodulin-intrinsic proteins in plant-*Rhizobium* symbioses (*17*, *18*). Once inside the highly acidic symbiosome, NH_3 will be immediately converted into NH_4^+, which cannot move across the plasma membrane, or through ayRhp1. This mechanism is known as "NH_4^+ acid trapping" and is well documented in diverse excretory epithelia from humans (*20*), teleost fishes (*39*), cephalopod and bivalve mollusks (*38*, *50*), and crustaceans [reviewed in (*26*); (*20*, *38*, *39*, *50*)]. Moreover, the uptake of NH_4^+ by the alga will ensure the continuous conversion of NH_3 into NH_4^+ in the symbiosome, which in turn will maintain NH_3 diffusion from the host cytosol. By analogy to the CCM that facilitates symbiont photosynthesis (*4*), NH_3 transport by ayRhp1 coupled to acid trapping of NH_4^+ in the symbiosome can be considered a host-controlled nitrogen concentrating mechanism (NCM). The high degree of conservation among cnidarian Rh channels (fig. S1) and the presence of an acidic symbiosome in anemones and corals from both the complex and robust clades (*4*) suggest that Rh-mediated NCMs are widespread in cnidarians. However, species- and environment-specific differences in the NCM contribution to Tamm transport may exist and must be explored.

In addition, CO_2-facilitated diffusion by ayRhp1 has implications for the host-controlled symbiosomal CCM (*4*). In this model, H^+ transport by VHA generates an acidic symbiosome that drives the DIC equilibrium toward CO_2 accumulation in the symbiosome space, which then diffuses into the alga where it is fixed by algal Rubisco. The presence of ayRhp1 in the symbiosome membrane may initially seem counterproductive for the CCM, as it provides a pathway for CO_2 to leak back into the host cell cytoplasm. Continued carbon fixation by the algae, however, ensures a more favorable gradient for CO_2 diffusion into the algae compared with the host cell. The CO_2 that backflows into the coral host cell would be hydrated by cytosolic carbonic anhydrases (CA) into H^+ and HCO_3^- (*51*), which can then be used as substrates for VHA and HCO_3^- transporters in the symbiosome membrane. Furthermore, the fluid in the coelenteron and mitochondria in the gastrodermal cells (*4*) are additional sources of CO_2 that can fuel symbiosome acidification (Fig. 5). This mechanism is akin to the human kidney collecting duct, where VHA, CAs, HCO_3^- transporters, and Rh channels interact with each other for the purposes of HCO_3^- reabsorption and Tamm excretion (*52*).

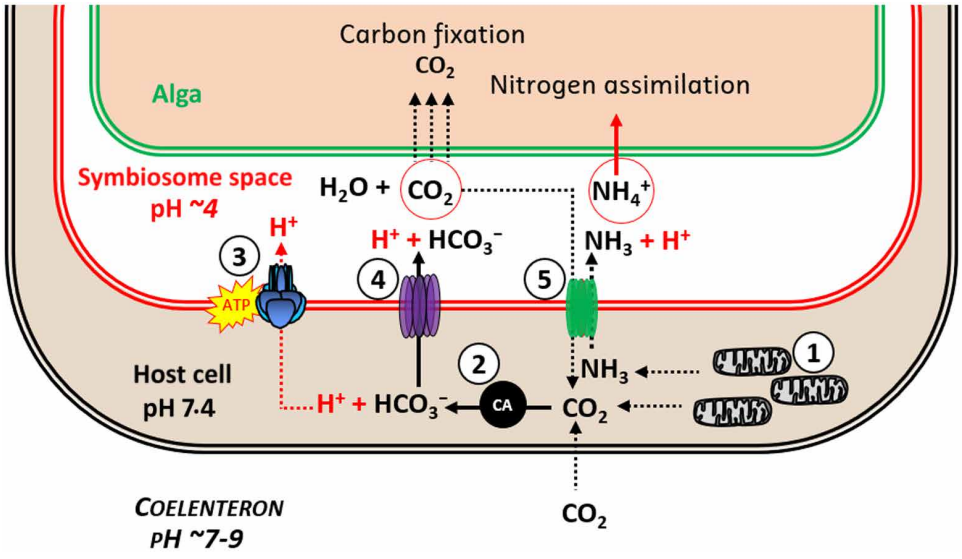

Fig. 5. Model of the coral nitrogen concentrating mechanism in alga-containing coral host cells. (**1**) Coral mitochondria produce NH_3 and CO_2. (**2**) Cytosolic CA catalyzes CO_2 hydration into H^+ and HCO_3^-. (**3**) H^+ and (**4**) HCO_3^- are moved into the symbiosome space by VHA and an unidentified HCO_3^- transporter, respectively. Inside the symbiosome, H^+ and HCO_3^- dehydrate into CO_2, which diffuses into and is photosynthetically fixed by the alga. (**5**) NH_3 diffuses via the *A. yongei* Rhesus protein (ayRhp1) into the symbiosome space, where it is immediately protonated and trapped as NH_4^+. An unidentified algal transporter imports NH_4^+ into the alga, where it is assimilated. Some CO_2 also diffuses via ayRhp1 back into the host cell's cytosol, where it is rehydrated and transported back to the symbiosome space. ATP, adenosine 5′-triphosphate.

The increased proportion of cells displaying symbiosomal ayRhp1 localization during the day matches established patterns of increased Tamm delivery from host to symbiont (*53*) and symbiont nitrogen assimilation (*9*) during light conditions. The diurnal nitrogen supply is primarily used not to advance growth but to sustain a high turnover of photosystem proteins and pigments damaged by ultraviolet radiation and electron transfer, which is essential for continued and efficient photosynthesis (*9*, *54*, *55*). This situation highlights the need for unique regulatory mechanisms in photosymbiotic associations compared with symbioses with nonphotosymbiotic microbes, such as those in plant roots. Conversely, the removal of ayRhp1 from the symbiosome membrane at night would serve to restrict nitrogen supply to symbiotic algae, thus limiting the synthesis of nonphotosynthetic proteins that would be essential to sustain their growth and reproduction (*55*). This mechanism gains additional significance when we consider that the coral symbiosome is highly acidic in both light and dark conditions (*4*), and this implies a continued steep inwardly directed pNH_3 gradient. Moreover, alga-containing gastrodermal cells are in contact with the gastrovascular cavity or coelenteron. This compartment contains Tamm at concentrations that can be several hundred-fold higher compared with seawater (*56*) and experiences steep diel pH fluctuations that can reach pH values as high as 9 during the day and as low as 6.75 at night (*56*, *57*). The presence of ayRhp1 channels in the host plasma membrane at night would facilitate the removal of NH_3 from the host cell into the coelenteron, where it would be trapped as NH_4, further restricting nitrogen supply to the algae at night.

The regulation of nitrogen delivery via changes in ayRhp1 subcellular localization is not mutually exclusive with regulation via the GS/GDH/GOGAT pathway (*11*, *58*, *59*), and they complement each other. The involvement of this pathway is largely based on changes in gene expression or enzyme activity upon transitioning from symbiotic to aposymbiotic stages (*22*) or during long-term environmental disturbances (*60*, *61*). But despite diel mRNA expression patterns (*62*), the abundance of most metabolic enzymes in coral cells, including that of GS, does not seem to change on a diel basis (*63*). However, this does not preclude diel regulation of enzyme activity by posttranslational modifications or substrate availability that could act synergistically with ayRhp1 to control nitrogen to symbiotic algae. Moreover, ayRhp1 subcellular localization was not identical in all cells at any time period, indicating finer regulation based on position on the coral colony, symbiotic stage, or some other unidentified factors.

Perspectives and limitations

The ayRhp1- and VHA-dependent NCM identified here together with diel changes in ayRhp1 subcellular distribution provide a potential mechanism whereby coral host cells can supply nitrogen to their algal symbionts while still maintaining them in a nitrogen-limited state to control their growth under oligotrophic conditions. Alterations in nitrogen delivery to coral symbiotic algae have been linked to eutrophication and other environmental stressors that result in disruption of the symbiosis at the colony level, commonly known as coral bleaching (*64*–*69*). For example, heat stress may promote coral amino acid catabolism as a means to meet increased metabolic demand in a warmed environment, which has been suggested to trigger a feedback loop that releases symbionts from nitrogen limitation, uncouples the symbiotic relationship, and leads to bleaching (*70*). In addition, future studies must take into account that ayRhp1 is present in multiple cell types throughout coral tissues, which cannot be discerned using transcriptomics, proteomics, or metabolomics assays on bulk coral colony samples. Specifically, changes in ayRhp1 abundance could be driven by ayRhp1 in cells in the epidermis, gastrodermis, calicodermis, or combinations, and each of these conditions would reflect a unique coral response, in some cases with opposite implications for coral health. With this in mind, techniques that allow

the investigation of coral biology at the cellular and molecular levels such as nanoscale secondary ion mass spectrometry ("nano-SIMS") (*11*, *70*) and confocal microscopy (*71*–*73*) are essential complements to "-omics" techniques. In particular, confocal Airyscan microscopy will allow studying physiological processes in calcifying cells and at the symbiosome membrane in unprecedent detail. Further work is required to determine whether the observed ayRhp1 symbiosomal localization is widespread among scleractinian corals. In addition, future studies should examine wild corals to ascertain the importance of this putative Rh channel–dependent NCM in the field. Future studies could also explore the role of other environmental nitrogen sources (i.e., urea and NO_3^-) on host-symbiont metabolism. These are time- and materials-intensive tasks but are necessary to fully contextualize the coral NCM at the ecophysiological level.

METHODS

Organisms

A. yongei colonies were maintained in flow-through seawater at 26°C with a 10/14-hour light/dark cycle with sunrise at 0800 and sunset at 1800. These coral colonies predominantly contain *Cladocopium* species (formerly *Symbiodinium* clade C). See the Supplementary Materials and Methods for additional information on coral husbandry.

Cloning of *ayRhp1*

Following the methods of (*15*), total RNA was collected by flash-freezing a 2-cm *A. yongei* nubbin in liquid nitrogen and crushing with a mortar and pestle into a fine powder. Powdered tissue was resuspended in TRIzol reagent (Invitrogen, Carlsbad, CA, USA), and total RNA was extracted following the manufacturer's protocol. Total RNA was cleaned and concentrated using an RNeasy Plus Mini Kit (Qiagen, Hilden, Germany). cDNA was synthesized using Super-Script III Reverse Transcriptase (Invitrogen) and Oligo(dT) primers according to the manufacturer's protocol. The resulting cDNA was used as template for all RT-PCRs. The full-length *ayRhp1* sequence was obtained and can be found on GenBank (MH025799).

Protein sequences for the phylogenetic analysis were sourced from (*74*) and GenBank via BLASTtn search. Accession numbers of all Rh sequences used in this analysis can be found in the supporting information file (Table S1).

Plasmid preparation and cDNA synthesis for *Xenopus laevis* expression of *ayRhp1*

The open reading frame of *ayRhp1* was amplified from pCR2.1 TOPO-*ayRhp1* vector (see cloning of ayRhp1) using Q5 high-fidelity DNA polymerase (New England Biolabs, Ipswich, MA, USA) and the restriction site–containing primers (forward primer, 5′-ATAC-CCGGGATGTCTACTCGACCTCCTACG-3′; reverse primer: 5′-GGCAAGCTTTTACACTTTATCATCTCCGAC-3′), subcloned by sticky-end ligation with T4 ligase (New England Biolabs) into Xma I and Hind III restriction sites of a pGEM-HE vector containing *Xenopus* beta globin 5′- and 3′-UTR sequences flanking the cloning site. Proper insertion was verified by restriction digest using Eco R1, Bam HI, and Sph I and visualized by gel electrophoresis to confirm *ayRhp1* fragments produced were of the expected size. The pGEM-HE vector containing the *ayRhp1* insert was linearized using Sph I; the restriction enzyme was heat inactivated at 65°C and linear plasmid column purified (GeneJet PCR Purification Kit; Thermo Fisher Scientific, Waltham, MA, USA). The in vitro transcription of *ayRhp1* capped mRNA (cRNA) was performed with HiScribe T7 ARCA mRNA kit (New England Biolabs) on Sph I linearized pGEM-HE-*ayRhp1* vector followed by column purification (RNeasy MiniElute Cleanup Kit; Qiagen). The cRNA was quantified spectrophotometrically (NanoDrop, ND-1000; Thermo Fisher Scientific), and its integrity was assessed on a denaturing MOPS agarose gel.

Oocyte microinjection

Stage VI–V oocytes were collected from mature female *X. laevis* (*75*). Briefly, the frogs were euthanized via decapitation, and the ovary was dissected and placed in Ca^{2+}-free oocyte ringer (OR2) solution (82.5 mM NaCl, 2.5 mM KCl, 1 mM $MgCl_2$, 1 mM Na_2HPO_4, 5 mM HEPES, pH 7.5) containing collagenase type VI (1 mg ml^{-1}; Thermo Fisher Scientific). After incubation under gentle agitation for 90 min at room temperature, collagenase activity was terminated by rinsing the oocytes three times in OR2 containing 1 mM $CaCl_2$. Oocytes were then manually sorted, rinsed, and allowed to recover in OR2 sterilized using vacuum bottle-top filters (EMD Millipore Steritop) overnight at 16°C (Fisherbrand Mini Refrigerated Incubator). Oocytes were injected with 18.4 ng of ayRhp1 cRNA (36.8 nl with 0.5 ng nl^{-1}) (ayRhp1) or equivalent volume of nuclease-free water (control) using a Nanoject II or III auto-nanoliter injector (Drummond Scientific, Broomall, PA, USA). Experiments were conducted 3 days postinjection; during this time, the oocytes were stored in OR2 supplemented with 2.5 mM sodium pyruvate, penicillin-streptomycin (1 mg ml^{-1}), and gentamicin (50 μg ml^{-1}). Oocytes that died during experiments were discounted from analyses. All procedures followed the Guidelines of the Canadian Council on Animal Care and were approved by the University of Manitoba Animal Research Ethics Board.

Oocyte Tamm uptake rates

Groups of control (water-injected) or ayRhp1 (ayRhp1 cRNA-injected) oocytes (24 oocytes = 1 replicate; $n = 6$ to 8) were placed in 15-ml tubes and incubated for 1 hour at room temperature in OR2 solutions containing (a) 0 mM NH_4Cl, pH 7.5; (b) 1 mM NH_4Cl, pH 6.5; (c) 1 mM NH_4Cl, pH 7.5; (d) 1 mM NH_4Cl, pH 8.5; or (e) 10 mM NH_4Cl, pH 7.5. Osmolarity was maintained by substituting NaCl with NH_4Cl, and pH was adjusted by adding NaOH or HCl. Following incubation, oocytes were washed in ice-cold OR2 to remove excess NH_4Cl and placed in groups of three oocytes in 27 μl of 6% perchloric acid to deproteinize samples (*76*). After pH neutralization with 3 M KOH, samples were diluted 1:10–1:40 with MilliQ water, and Tamm was measured using a hypochlorite-salicylate-nitroprusside–based assay (*77*). Tamm uptake rate was calculated according to the formula

$$\text{Tamm uptake rate} = \frac{[\text{Tamm}]_{t=1\text{h}} - [\text{Tamm}]_{t=0\text{h}}}{1\ \mu\text{l} \times 60\ \text{min}}$$

where $[\text{Tamm}]_{t=1\text{h}}$ is the Tamm measured in oocytes after incubation in OR2 (b) to (e) for 1 hour, $[\text{Tamm}]_{t=0\text{h}}$ is Tamm measured in oocytes in OR2 (a) before the start of the incubations, 1 μl is the average oocyte volume, and 60 min was used to calculate rates on a per minute basis. The average Tamm uptake rate of control oocytes was subtracted from that of ayRhp1 oocytes before statistical analysis (fig. S3). Tamm uptake kinetics were calculated using a nonlinear regression to fit the Michaelis-Menten equation.

Oocyte CO_2 release rates

Hypercapnic OR2 was generated by aeration with 5% CO_2 until pH reached equilibrium. Groups of control or ayRhp1 oocytes

(25 oocytes = 1 replicate; $n = 8$) were incubated in 40 ml of hypercapnic OR2 for 1.5 hours at 16°C. Oocytes were transferred along with hypercapnic OR2 into 2-ml septum capped gas tight vials. Hypercapnic OR2 was sequentially removed from each vial, replaced with normocapnic OR2, and sealed while submerged in OR2 to prevent air bubbles. Rapid transfer from hypercapnic to normocapnic OR2 was used to generate an oocyte-to-OR2 pCO_2 gradient. One minute after sealing the chambers, three replicate 5-µl samples were taken with a gas tight Hamilton syringe from the vial by piercing the septum on the cap and injected into a custom-built total CO_2 analyzer using a Licor 850 (LI-COR Biosciences, Lincoln, NE, USA) for CO_2 detection as previously described (*36*). Standards of 0, 0.2, 0.3, 0.4, and 0.5 mmol l^{-1} $NaHCO_3$ were used to calibrate the CO_2 analyzer and produced an R^2 of 0.99. CO_2 release rate was calculated according to the formula

$$CO_2 \text{ release rate} = \frac{\left(\frac{CO_2 \text{ release}_{t=1\text{min}}\ \mu\text{mol} - 0.4644}{0.1960}\right) \times 0.002\ \text{L}}{25 \text{ oocytes} \times 1 \text{ min} \times \frac{1000 \text{ nmol}}{\mu\text{mol}}}$$

where $CO_2 \text{ release}_{t\,=\,1\text{min}}$ is the CO_2 measured in the sample after 1 min of incubation in normocapnic OR2, 0.04644 and 0.1960 are corrections calculated from the standard curve, 0.002 L is the chamber volume, 25 oocytes are the number of oocytes per chamber, and 1 min is the CO_2 flux period, The integrity of oocytes in all vials was confirmed under a microscope at the end of the sampling period.

Antibodies

Custom-made, affinity-purified anti-ayRhp1 rabbit polyclonal antibodies were developed (GenScript USA Inc., Piscataway, NJ, USA) against the peptide CHNKDAHGSHKEGSN, which is present in a putative Rhp1 protein predicted from the *Acropora digitifera* genome (XP_015769291.1) (*78*). This epitope has just one amino acid difference in ayRhp1 (CHNKDAHGS**P**KEGSN). NKA was immunolocalized with a commercially available monoclonal antibody (SC-48345, Santa Cruz Biotechnology, Dallas, TX, USA).

ayRhp1 protein expression and antibody validation

Using methods adapted from (*4*), *A. yongei* tissue was removed from the skeleton using an airbrush loaded with homogenization buffer. Briefly, homogenate was sonicated on ice and centrifuged to pellet down debris; the supernatant was kept on ice. Sample protein concentrations were determined using a Bradford Protein Assay (Bio-Rad, Hercules, CA, USA) with a bovine serum albumin standard curve. Samples were then incubated in 4× Laemmli sample buffer (Bio-Rad) and 10% β-mercaptoethanol before heating at 90°C for 3 min and loaded onto an SDS–polyacrylamide gel electrophoresis (PAGE) gel. Following electrophoresis, proteins were transferred from the gel onto a polyvinylidene difluoride (PVDF) membrane using a Mini Tans-Blot Cell (Bio-Rad) overnight. The membrane was blocked with 5% powdered fat-free milk in TBS-T for 1 hour on a shaker at room temperature before overnight incubation on a shaker (4°C) with anti-ayRhp1 primary antibody (0.216 µg ml^{-1}), primary antibody with 400× excess peptide on a molar base ("preabsorption control"), or preimmune serum (0.216 µg ml^{-1}) diluted in blocking buffer. Membranes were washed with 4 × 15 min TBS-T washes before incubation with secondary antibody [goat anti–rabbit–horseradish peroxidase (HRP) diluted 1:10,000, Bio-Rad] for 1 hour on a shaker at room temperature. Membranes were again washed with 4 × 15 min TBS-T washes and a final 15-min TBS wash before band development with an ECL Prime Western blot Detection Kit (GE Healthcare, Chicago, IL, USA) and imaged using a Chemidoc Imaging system (Bio-Rad) (fig. S4D). See the Supplementary Materials and Methods for additional information.

Immunofluorescence

Some *A. yongei* nubbins were fixed and decalcified, and others were brushed with a toothbrush to isolate cells prior to fixing following previously described methods (*4*, *15*, *49*, *71*, *73*) (see the Supplementary Materials and Methods for details). Tissue sections and isolated cells were incubated for 1 hour at room temperature in blocking buffer [4 ml of phosphate-buffered saline with Triton X-100 (PBS-TX), 80 µl of normal goat serum, and 0.8 µl of keyhole limpet hemocyanin solution], followed by overnight incubation (4°C) with anti-ayRhp1 antibodies (2.16 µg ml^{-1}), anti-ayRhp1 antibodies preabsorbed with excess peptide (8.64 µg ml^{-1}), or preimmune serum (2.16 µg ml^{-1}) alone or in combination with the anti-NKA antibody (2.00 µg ml^{-1}) (all in blocking buffer) (fig. S4, A to C).

Slides were washed in PBS-TX to remove unbound primary antibodies (3 × 5 min). Secondary antibodies (goat anti–rabbit–Alexa Fluor 555, goat anti–rabbit–Alexa Fluor 488, and/or goat anti–mouse–Alexa Fluor568, 4 µg/ml in blocking buffer; Invitrogen) were then added for 1 hour at room temperature followed by 4′,6-diamidino-2-phenylindole (DAPI) DNA stain (1 µg ml^{-1} in blocking buffer; Invitrogen) for 5 min at room temperature and washed again in PBS-TX to remove unbound secondary antibodies and DAPI (3 × 5 min).

Epifluorescence microscopy was performed on a Zeiss AxioObserver Z1 (Carl Zeiss AG, Oberkochen, Germany) connected to a metal halide lamp. ayRhp1 and DAPI signals in tissue sections (Fig. 2 and fig. S4, A to C_1) were visualized using HE Cy3 [excitation (ex): 550 nm, emission (em): 570 nm] and DAPI (ex: 359 nm, em: 461 nm) filters, respectively. ayRhp1 and DAPI signals in isolated cells (fig. S5) were visualized using HE DsRed (ex: 538 to 562 nm, em: 570 to 640 nm) and FURA (ex: 335 to 345 and 375 to 385 nm, em: 505 to 530 nm) filters, respectively.

Confocal Airyscan microscopy was performed on a Zeiss AxioObserver Z1 connected to a laser scanner equipped with 405-, 488-, 561-, and 640-nm laser lines (Zeiss LSM 800 with Airyscan, Carl Zeiss AG). This device uses a 32-channel photomultiplier detector and linear deconvolution to obtain 140-nm lateral (*X*-*Y*) and 400-nm axial (*Z*) resolution. ayRhp1, NKA, and DAPI signals in tissue sections (Figs. 4, A and B, and 3) were visualized using goat anti–rabbit–Alexa Fluor 488 and goat anti–mouse–Alexa Fluor568 secondary antibodies (Invitrogen) and DAPI stain (Invitrogen), respectively (Alexa Fluor 488—ex: 517 nm, em: 497 to 574 nm; Alexa Fluor 568—ex: 577 nm, em: 560 to 643 nm; DAPI—ex: 465 nm, em: 400 to 484 nm). Three-dimensional reconstructions of *z*-stacks were generated using Imaris 9.0 (Bitplane, Zurich, Switzerland). To facilitate visualization by color-blind readers, NKA, ayRhp1, and DAPI signals are presented using the false colors violet, green, and blue, respectively, in all figures.

Assessment of ayRhp1 subcellular localization over day-night cycles

Cell isolations were prepared from coral nubbins randomly selected from three separate tanks. Nubbins were sampled 30 min before and after sunrise and sunset (0730, 0830, 1730, and 1830 hours) as

well as halfway between lighting condition changes (1300 and 2300 hours). Samples taken during the day were continually illuminated during cell isolation and fixation, while those taken during the night were kept in the dark. At each time point, cells were immunostained for ayRhp1 and imaged as described above. Starting from the upper-right corner of the field of view, the first 50 intact alga-hosting *A. yongei* cells displaying ayRhp1 signal were counted and classified into one of two subcellular localization patterns: "symbiosomal ayRhp1 localization" (the ayRhp1 signal clearly traversed the region between the nuclei of the coral host cell and the algae) or nonsymbiosomal localization (ayRhp1 signal was absent from this region but present exterior and adjacent to the host nucleus). Cells were counted and classified in a double-blind manner: Slides were named with random identifiers by an independent person before being observed on the fluorescence microscope by another person. Classification was conducted during observation through the microscope eyepiece, as this allowed a better determination of ayRhp1 subcellular localization by rapid and repetitive adjustments to the fine focus and alternation between the Alexa Fluor 555 and DAPI channels. Cells from three separate branches were classified at each time point, resulting in a total of 150 cells per time point and 900 cells in total. Time points were matched with random slide names only once all 900 cells were classified. Raw count data are presented in data S1.

Statistical analysis

All statistical tests were run in GraphPad Prism 7 (San Diego, CA, USA). Tamm uptake, CO_2 release, and ayRhp1 localization data were tested for normality and homogeneity of variance using D'Agostino and Pearson or Shapiro-Wilk normality tests and Brown-Forsythe tests. Tamm uptake data were analyzed using one-way analysis of variance (ANOVA) with Tukey's multiple comparisons. CO_2 release data were analyzed using a Welch's *t* test (two-tailed, unequal variance). Data from ayRhp1 localization in isolated cells were analyzed using two-way repeated-measures ANOVA followed by Dunnett's posttest using the data from 1300 hours as control. Alpha was set at 0.05 for all statistical tests.

SUPPLEMENTARY MATERIALS

Supplementary material for this article is available at https://science.org/doi/10.1126/sciadv.abm0303

View/request a protocol for this paper from *Bio-protocol*.

REFERENCES AND NOTES

1. M. J. H. van Oppen, M. Medina, Coral evolutionary responses to microbial symbioses. *Philos. Trans. R. Soc. Lond. B Biol. Sci.* **375**, 20190591 (2020).
2. Y. Tanaka, A. Suzuki, K. Sakai, The stoichiometry of coral-dinoflagellate symbiosis: Carbon and nitrogen cycles are balanced in the recycling and double translocation system. *ISME J.* **12**, 860–868 (2018).
3. B. L. Tang, Thoughts on a very acidic symbiosome. *Front. Microbiol.* **6**, 816 (2015).
4. K. L. Barott, A. A. Venn, S. O. Perez, S. Tambutté, M. Tresguerres, Coral host cells acidify symbiotic algal microenvironment to promote photosynthesis. *Proc. Natl. Acad. Sci. U.S.A.* **112**, 607–612 (2015).
5. O. Rahav, Z. Dubinsky, Y. Achituv, P. G. Falkowski, Ammonium metabolism in the zooxanthellate coral, *Stylophora pistillata*. *Proc. R. Soc. Lond. B.* **236**, 325–337 (1989).
6. P. A. Wright, Nitrogen excretion: Three end products, many physiological roles. *J. Exp. Biol.* **198**, 273–281 (1995).
7. A. M. Szmant, L. M. Ferrer, L. M. FitzGerald, Nitrogen excretion and O:N ratios in reef corals: Evidence for conservation of nitrogen. *Mar. Biol.* **104**, 119–127 (1990).
8. G. Cui, Y. J. Liew, Y. Li, N. Kharbatia, N. I. Zahran, A. H. Emwas, V. M. Eguiluz, M. Aranda, Host-dependent nitrogen recycling as a mechanism of symbiont control in *Aiptasia*. *PLOS Genet.* **15**, e1008189 (2019).
9. C. Kopp, M. Pernice, I. Domart-Coulon, C. Djediat, J. E. Spangenberg, D. T. L. Alexander, M. Hignette, T. Meziane, A. Meibom, Highly dynamic cellular-level response of symbiotic coral to a sudden increase in environmental nitrogen. *mBio* **4**, e00052-13 (2013).
10. C. D'Elia, S. Domotor, K. Webb, Nutrient uptake kinetics of freshly isolated zooxanthellae*. *Mar. Biol.* **167**, 157–167 (1983).
11. M. Pernice, A. Meibom, A. Van Den Heuvel, C. Kopp, I. Domart-Coulon, O. Hoegh-Guldberg, S. Dove, A single-cell view of ammonium assimilation in coral-dinoflagellate symbiosis. *ISME J.* **6**, 1314–1324 (2012).
12. T. A. V. Rees, Are symbiotic algae nutrient deficient? *Proc. R. Soc. B Biol. Sci.* **243**, 227–233 (1991).
13. T. Krueger, N. Horwitz, J. Bodin, M. E. Giovani, S. Escrig, M. Fine, A. Meibom, Intracellular competition for nitrogen controls dinoflagellate population density in corals. *Proc. Biol. Sci.* **287**, 20200049 (2020).
14. A. E. Sproles, N. L. Kirk, S. A. Kitchen, C. A. Oakley, A. R. Grossman, V. M. Weis, S. K. Davy, Phylogenetic characterization of transporter proteins in the cnidarian-dinoflagellate symbiosis. *Mol. Phylogenet. Evol.* **120**, 307–320 (2018).
15. K. L. Barott, M. E. Barron, M. Tresguerres, Identification of a molecular pH sensor in coral. *Proc. R. Soc. B* **284**, 20171769 (2017).
16. I. D. Weiner, J. W. Verlander, Ammonia transporters and their role in acid-base balance. *Physiol. Rev.* **97**, 465–494 (2017).
17. I. S. Wallace, W.-G. Choi, D. M. Roberts, The structure, function and regulation of the nodulin 26-like intrinsic protein family of plant aquaglyceroporins. *Biochim. Biophys. Acta* **1758**, 1165–1175 (2006).
18. C. M. Niemietz, S. D. Tyerman, Channel-mediated permeation of ammonia gas through the peribacteroid membrane of soybean nodules. *FEBS Lett.* **465**, 110–114 (2000).
19. R. R. Geyer, M. D. Parker, A. M. Toye, W. F. Boron, R. Musa-Aziz, Relative CO_2/NH_3 permeabilities of human RhAG, RhBG and RhCG. *J. Membr. Biol.* **246**, 915–926 (2013).
20. F. Gruswitz, S. Chaudhary, J. D. Ho, A. Schlessinger, B. Pezeshki, C.-M. Ho, A. Sali, C. M. Westhoff, R. M. Stroud, Function of human Rh based on structure of RhCG at 2.1 A. *Proc. Natl. Acad. Sci. U.S.A.* **107**, 9638–9643 (2010).
21. S. Baday, E. A. Orabi, S. Wang, G. Lamoureux, S. Bernèche, Mechanism of NH_4^+ recruitment and NH_3 transport in Rh proteins. *Structure* **23**, 1550–1557 (2015).
22. E. M. Lehnert, M. E. Mouchka, M. S. Burriesci, N. D. Gallo, J. A. Schwarz, J. R. Pringle, Extensive differences in gene expression between symbiotic and aposymbiotic cnidarians. *G3* **4**, 277–295 (2014).
23. Y. Ishii, S. Maruyama, H. Takahashi, Y. Aihara, T. Yamaguchi, K. Yamaguchi, S. Shigenobu, M. Kawata, N. Ueno, J. Minagawa, Global shifts in gene expression profiles accompanied with environmental changes in cnidarian-dinoflagellate endosymbiosis. *G3* **9**, 2337–2347 (2019).
24. P. Ganot, A. Moya, V. Magnone, D. Allemand, P. Furla, C. Sabourault, Adaptations to endosymbiosis in a Cnidarian-Dinoflagellate association: Differential gene expression and specific gene duplications. *PLOS Genet.* **7**, e1002187 (2011).
25. M. Hu, X. Zheng, C.-M. Fan, Y. Zheng, Lineage dynamics of the endosymbiotic cell type in the soft coral *Xenia*. *Nature* **582**, 534–538 (2020).
26. D. Weihrauch, M. O'Donnell, *Acid-Base Balance and Nitrogen Excretion in Invertebrates* (Springer International Publishing, 2017); http://link.springer.com/10.1007/978-3-319-39617-0.
27. M. Benghezal, D. Gotthardt, S. Cornillon, P. Cosson, Localization of the Rh50-like protein to the contractile vacuole in *Dictyostelium*. *Immunogenetics* **52**, 284–288 (2001).
28. K. H. Han, K. Mekala, V. Babida, H. Y. Kim, M. E. Handlogten, J. W. Verlander, I. D. Weiner, Expression of the gas-transporting proteins, Rh B glycoprotein and Rh C glycoprotein, in the murine lung. *Am. J. Physiol. Lung Cell. Mol. Physiol.* **297**, L153–L163 (2009).
29. S. F. Perry, M. H. Braun, M. Noland, J. Dawdy, P. J. Walsh, Do zebrafish Rh proteins act as dual ammonia-CO2 channels? *J. Exp. Zool. A Ecol. Genet. Physiol.* **313**, 618–621 (2010).
30. V. Endeward, J. P. Cartron, P. Ripoche, G. Gros, RhAG protein of the Rhesus complex is a CO2 channel in the human red cell membrane. *FASEB J.* **22**, 64–73 (2008).
31. C. M. Nawata, C. M. Wood, M. J. O'Donnell, Functional characterization of Rhesus glycoproteins from an ammoniotelic teleost, the rainbow trout, using oocyte expression and SIET analysis. *J. Exp. Biol.* **213**, 1049–1059 (2010).
32. X.-D. Li, D. Lupo, L. Zheng, F. Winkler, Structural and functional insights into the AmtB/Mep/Rh protein family. *Transfus. Clin. Biol.* **13**, 65–69 (2006).
33. J. Stolarski, M. V. Kitahara, D. J. Miller, S. D. Cairns, M. Mazur, A. Meibom, The ancient evolutionary origins of Scleractinia revealed by azooxanthellate corals. *BMC Evol. Biol.* **11**, 316 (2011).
34. A. M. Marini, M. Boeckstaens, F. Benjelloun, B. Chérif-Zahar, B. André, Structural involvement in substrate recognition of an essential aspartate residue conserved in Mep/Amt and Rh-type ammonium transporters. *Curr. Genet.* **49**, 364–374 (2006).
35. X. Li, S. Jayachandran, H.-H. H. T. Nguyen, M. K. Chan, Structure of the *Nitrosomonas europaea* Rh protein. *Proc. Natl. Acad. Sci. U.S.A.* **104**, 19279–19284 (2007).
36. D. J. Lee, M. Gutbrod, F. M. Ferreras, P. G. D. Matthews, Changes in hemolymph total CO_2 content during the water-to-air respiratory transition of amphibiotic dragonflies. *J. Exp. Biol.* **221**, jeb181438 (2018).

37. S. Sasaki, K. Ishibashi, T. Nagai, F. Marumo, Regulation mechanisms of intracellular pH of *Xenopus laevis* oocyte. *Biochim. Biophys. Acta* **1137**, 45–51 (1992).
38. J. Thomsen, N. Himmerkus, N. Holland, F. J. Sartoris, M. Bleich, M. Tresguerres, Ammonia excretion in mytilid mussels is facilitated by ciliary beating. *J. Exp. Biol.* **219**, 2300–2310 (2016).
39. P. A. Wright, C. M. Wood, A new paradigm for ammonia excretion in aquatic animals: Role of Rhesus (Rh) glycoproteins. *J. Exp. Biol.* **212**, 2303–2312 (2009).
40. D. Thiel, M. Hugenschutt, H. Meyer, A. Paululat, A. R. Quijada-Rodriguez, G. Purschke, D. Weihrauch, Ammonia excretion in the marine polychaete Eurythoe complanata (Annelida). *J. Exp. Biol.* **220**, 425–436 (2017).
41. J. G. Tidball, Fine structural aspects of anthozoan desmocyte development (Phylum Cnidaria). *Tissue Cell* **14**, 85–96 (1982).
42. L. Muscatine, E. Tambutte, D. Allemand, Morphology of coral desmocytes, cells that anchor the calicoblastic epithelium to the skeleton. *Coral Reefs* **16**, 205–213 (1997).
43. J. W. Campbell, K. V. Speeg, Ammonia and biological deposition of calcium carbonate. *Nature* **224**, 725–726 (1969).
44. R. A. Loest, Ammonia-forming enzymes and calcium-carbonate deposition in terrestrial pulmonates. *Physiol. Zool.* **52**, 470–483 (1979).
45. C. J. Crossland, D. J. Barnes, The role of metabolic nitrogen in coral calcification. *Mar. Biol.* **28**, 325–332 (1974).
46. W. J. Cai, Y. Ma, B. M. Hopkinson, A. G. Grottoli, M. E. Warner, Q. Ding, X. Hu, X. Yuan, V. Schoepf, H. Xu, C. Han, T. F. Melman, K. D. Hoadley, D. T. Pettay, Y. Matsui, J. H. Baumann, S. Levas, Y. Ying, Y. Wang, Microelectrode characterization of coral daytime interior pH and carbonate chemistry. *Nat. Commun.* **7**, 11144 (2016).
47. N. Allison, I. Cohen, A. A. Finch, J. Erez, A. W. Tudhope, Corals concentrate dissolved inorganic carbon to facilitate calcification. *Nat. Commun.* **5**, 5741 (2014).
48. J. H. Kaplan, Biochemistry of Na,K-ATPase. *Annu. Rev. Biochem.* **71**, 511–535 (2002).
49. A. A. Venn, E. Tambutté, S. Lotto, D. Zoccola, D. Allemand, S. Tambutté, Imaging intracellular pH in a reef coral and symbiotic anemone. *Proc. Natl. Acad. Sci. U.S.A.* **106**, 16574–16579 (2009).
50. M. Y. Hu, Y. J. Guh, M. Stumpp, J. R. Lee, R. D. Chen, P. H. Sung, Y. C. Chen, P. P. Hwang, Y. C. Tseng, Branchial NH_4^+-dependent acid-base transport mechanisms and energy metabolism of squid (*Sepioteuthis lessoniana*) affected by seawater acidification. *Front. Zool.* **11**, 55 (2014).
51. A. Bertucci, A. Moya, S. Tambutté, D. Allemand, C. T. Supuran, D. Zoccola, Carbonic anhydrases in anthozoan corals - a review. *Bioorg. Med. Chem.* **21**, 1437–1450 (2013).
52. I. D. Weiner, J. W. Verlander, Renal ammonia metabolism and transport. *Compr. Physiol.* **3**, 201–220 (2013).
53. R. Grover, J.-F. Maguer, S. Reynaud-vaganay, C. Ferrier-Pagès, Uptake of ammonium by the scleractinian coral *Stylophora pistillata*: Effect of feeding, light, and ammonium concentrations. *Limnol. Oceanogr.* **47**, 782–790 (2002).
54. E. Beraud, F. Gevaert, C. Rottier, C. Ferrier-Pages, The response of the scleractinian coral Turbinaria reniformis to thermal stress depends on the nitrogen status of the coral holobiont. *J. Exp. Biol.* **216**, 2665–2674 (2013).
55. N. Rosic, P. Kaniewska, C.-K. Chan, E. Y. Ling, D. Edwards, S. Dove, O. Hoegh-Guldberg, Early transcriptional changes in the reef-building coral Acropora aspera in response to thermal and nutrient stress. *BMC Genomics* **15**, 1052 (2014).
56. S. Agostini, Y. Suzuki, T. Higuchi, B. E. Casareto, K. Yoshinaga, Y. Nakano, H. Fujimura, Biological and chemical characteristics of the coral gastric cavity. *Coral Reefs* **31**, 147–156 (2012).
57. P. Furla, I. Galgani, I. Durand, D. Allemand, Sources and mechanisms of inorganic carbon transport for coral calcification and photosynthesis. *J. Exp. Biol.* **203**, 3445–3457 (2000).
58. D. Yellowlees, T. A. V. Rees, W. Leggat, Metabolic interactions between algal symbionts and invertebrate hosts. *Plant. Cell Environ.* **31**, 679–694 (2008).
59. C. A. Oakley, M. F. Ameismeier, L. Peng, V. M. Weis, A. R. Grossman, S. K. Davy, Symbiosis induces widespread changes in the proteome of the model cnidarian *Aiptasia*. *Cell. Microbiol.* **18**, 1009–1023 (2016).
60. D. Yellowlees, T. Rees, W. Fitt, Effect of ammonium-supplemented seawater on glutamine synthetase and glutamate dehydrogenase activities in host tissue and zooxanthellae of Pocillopora damicornis and on ammonium uptake rates of the zooxanthellae. *Pacific Sci.* **48**, 291–295 (1994).
61. J. Tang, X. Ni, J. Wen, L. Wang, J. Luo, Z. Zhou, Increased ammonium assimilation activity in the scleractinian coral *Pocillopora damicornis* but not its symbiont after acute heat stress. *Front. Mar. Sci.* **7**, 565068 (2020).
62. O. Levy, P. Kaniewska, S. Alon, E. Eisenberg, S. Karako-Lampert, L. K. Bay, R. Reef, M. Rodriguez-Lanetty, D. J. Miller, O. Hoegh-Guldberg, Complex diel cycles of gene expression in coral-algal symbiosis. *Science* **331**, 175 (2011).
63. L. B. Linsmayer, D. D. Deheyn, L. Tomanek, M. Tresguerres, Dynamic regulation of coral energy metabolism throughout the diel cycle. *Sci. Rep.* **10**, 19881 (2020).
64. N. M. Kuntz, D. I. Kline, S. A. Sandin, F. Rohwer, Pathologies and mortality rates caused by organic carbon and nutrient stressors in three Caribbean coral species. *Mar. Ecol. Prog. Ser.* **294**, 173–180 (2005).
65. C. Schlöder, L. D'Croz, Responses of massive and branching coral species to the combined effects of water temperature and nitrate enrichment. *J. Exp. Mar. Biol. Ecol.* **313**, 255–268 (2004).
66. S. A. Wooldridge, T. J. Done, C. R. Thomas, I. I. Gordon, P. A. Marshall, R. N. Jones, Safeguarding coastal coral communities on the central Great Barrier Reef (Australia) against climate change: Realizable local and global actions. *Clim. Change* **112**, 945–961 (2012).
67. P. A. Cleves, C. J. Krediet, E. M. Lehnert, M. Onishi, J. R. Pringle, Insights into coral bleaching under heat stress from analysis of gene expression in a sea anemone model system. *Proc. Natl. Acad. Sci. U.S.A.* **117**, 28906–28917 (2020).
68. L. A. Morris, C. R. Voolstra, K. M. Quigley, D. G. Bourne, L. K. Bay, Nutrient availability and metabolism affect the stability of coral–*symbiodiniaceae* symbioses. *Trends Microbiol.* **27**, 678–689 (2019).
69. J. Wiedenmann, C. D'Angelo, E. G. Smith, A. N. Hunt, F. E. Legiret, A. D. Postle, E. P. Achterberg, Nutrient enrichment can increase the susceptibility of reef corals to bleaching. *Nat. Clim. Chang.* **3**, 160–164 (2013).
70. N. Rädecker, C. Pogoreutz, H. M. Gegner, A. Cárdenas, F. Roth, J. Bougoure, P. Guagliardo, C. Wild, M. Pernice, J. B. Raina, A. Meibom, C. R. Voolstra, Heat stress destabilizes symbiotic nutrient cycling in corals. *Proc. Natl. Acad. Sci. U.S.A.* **118**, e2022653118 (2021).
71. M. E. Barron, A. B. Thies, J. A. Espinoza, K. L. Barott, A. Hamdoun, M. Tresguerres, A vesicular Na+/Ca2+ exchanger in coral calcifying cells. *PLOS ONE* **13**, e0205367 (2018).
72. P. Ganot, E. Tambutté, N. Caminiti-Segonds, G. Toullec, D. Allemand, S. Tambutté, Ubiquitous macropinocytosis in anthozoans. *eLife* **9**, e50022 (2020).
73. K. L. Barott, A. A. Venn, A. B. Thies, S. Tambutté, M. Tresguerres, Regulation of coral calcification by the acid-base sensing enzyme soluble adenylyl cyclase. *Biochem. Biophys. Res. Commun.* **525**, 576–580 (2020).
74. C.-H. Huang, J. Peng, Evolutionary conservation and diversification of Rh family genes and proteins. *Proc. Natl. Acad. Sci.* **102**, 15512–15517 (2005).
75. H. Soreq, S. Seidman, *Xenopus* oocyte microinjection: From gene to protein. *Methods Enzymol.* **207**, 225–265 (1992).
76. C. M. Veauvy, P. J. Walsh, M. D. Mcdonald, Effect of elevated ammonia on tissue nitrogen metabolites in the ureotelic gulf toadfish (*Opsanus beta*) and the ammoniotelic midshipman (*Porichthys notatus*). *Physiol. Biochem. Zool.* **82**, 345–352 (2009).
77. A. J. Kempers, C. J. Kok, Re-examination of the determination of ammonium as the indophenol blue complex using salicylate. *Anal. Chim. Acta* **221**, 147–155 (1989).
78. C. Shinzato, E. Shoguchi, T. Kawashima, M. Hamada, K. Hisata, M. Tanaka, M. Fujie, M. Fujiwara, R. Koyanagi, T. Ikuta, A. Fujiyama, D. J. Miller, N. Satoh, Using the *Acropora digitifera* genome to understand coral responses to environmental change. *Nature* **476**, 320–323 (2011).
79. R. C. Edgar, MUSCLE: A multiple sequence alignment method with reduced time and space complexity. *BMC Bioinformatics* **5**, 113 (2004).
80. A. Stamatakis, RAxML version 8: A tool for phylogenetic analysis and post-analysis of large phylogenies. *Bioinformatics* **30**, 1312–1313 (2014).
81. E. L. Sonnhammer, G. von Heijne, A. Krogh, A hidden Markov model for predicting transmembrane helices in protein sequences. *Proc. Int. Conf. Intell. Syst. Mol. Biol.* **6**, 175–182 (1998).
82. A. Krogh, B. Larsson, G. Von Heijne, E. L. L. Sonnhammer, Predicting transmembrane protein topology with a hidden Markov model: Application to complete genomes. *J. Mol. Biol.* **305**, 567–580 (2001).
83. M. E. Jørgensen, H. H. Nour-Eldin, B. A. Halkier, in *Biotechnology of Plant Secondary Metabolism: Methods and Protocols*, A. G. Fett-Neto, Ed. (Springer Science & Business Media, 2016); http://link.springer.com/10.1007/978-1-4939-3393-8, vol. 1405, pp. 99–107.
84. K. Barott, M. Tresguerres, Immunolocalization of proteins in corals: The V-type H^+-ATPase proton pump. *Bio-protocol* **5**, e1573 (2015).

Acknowledgments: We thank M. Romero (Mayo Clinic) for the gift of *Xenopus* expression vector; M. Ortega, S. Nöel, A. Serna, C. Hassabi, D. Jio, and P. Zerofski (Scripps Institution of Oceanography) for help in maintaining coral cultures; and M. Nash (University of Manitoba) for support with oocyte sorting and maintenance. **Funding:** This work was partially supported by the National Science Foundation (NSF) EF #1220641 to M.T., NSF Graduate Research (GRFP 2019271478) and SIO Doctoral Scholar Fellowships to A.B.T., Natural Sciences and Engineering Research Council of Canada (NSERC) Postgraduate Doctoral Scholarship-Doctoral to A.R.Q.-R., University of Manitoba Graduate Fellowship to H.Z., and NSERC Discovery grant (RGPIN/5013-2018) to D.W. **Author contributions:** M.T. and A.B.T. conceived the project. M.T. and D.W. directed the research. A.B.T. performed all cloning, antibody validation, and microscopy experiments. A.R.Q.-R. and H.Z. performed oocyte experiments. A.B.T., A.R.Q.-R., D.W., and M.T. analyzed the data. A.B.T. and M.T. wrote the manuscript. All authors read and edited the manuscript. **Competing interests:** The authors declare that they have no competing interests. **Data and materials availability:** All data needed to evaluate the conclusions in the paper are present in the paper and/or the Supplementary Materials.

Submitted 25 August 2021
Accepted 20 January 2022
Published 11 March 2022
10.1126/sciadv.abm0303

ScienceAdvances

A Rhesus channel in the coral symbiosome membrane suggests a novel mechanism to regulate NH and CO delivery to algal symbionts

Angus B. ThiesAlex R. Quijada-RodriguezHaonan ZhouyaoDirk WeihrauchMartin Tresguerres

Sci. Adv., 8 (10), eabm0303.

Science Advances (ISSN) is published by the American Association for the Advancement of Science. 1200 New York Avenue NW, Washington, DC 20005. The title *Science Advances* is a registered trademark of AAAS.

Science Advances
AAAS

Supplementary Materials for

A Rhesus channel in the coral symbiosome membrane suggests a novel mechanism to regulate NH_3 and CO_2 delivery to algal symbionts

Angus B. Thies*, Alex R. Quijada-Rodriguez, Haonan Zhouyao,
Dirk Weihrauch, Martin Tresguerres*

*Corresponding author. Email: athies@ucsd.edu (A.B.T.); mtresguerres@ucsd.edu (M.T.)

Published 11 March 2022, *Sci. Adv.* **8**, eabm0303 (2022)
DOI: 10.1126/sciadv.abm0303

The PDF file includes:

Other Supplementary Material for this manuscript includes the following:

SI Methods

Organisms

A. yongei nubbins were originally sourced from the Birch Aquarium at Scripps and reared in a heated flow-through seawater aquaria at Scripps Institution of Oceanography for at least 1 year prior to the experiments. These coral colonies predominantly contain *Cladocopium sp* (formerly *Symbiodinium* clade C). Average [PO_4^{3-}], [NO_3^-], [NO_2^-] and [NH_4^+] were 0.35 ± 0.02 μM, 0.29 ± 0.11 μM, 0 μM and 0.54 ± 0.1 μM, respectively (Southern California Coastal Ocean Observing System; https://sccoos.org/harmful-algal-bloom/). Temperature was kept at 26°C, light/dark cycle was 10/14h with sunrise at 08:00 and sunset at 18:00 (LED Fixture lights, Orbit Marine, model 4103-B). Light intensity in the aquaria was measured to be 120 μE (MSC15 Spectral Light Meter, Gigahertz-Optik, Amesbury, MA, USA).

Cloning of ayRhp1

Following the methods of (*15*), total RNA was collected by flash-freezing a 2cm *A. yongei* nubbin in liquid nitrogen and crushing with a mortar and pestle into a fine powder. Powdered tissue was resuspended in TRIzol reagent (Invitrogen, Carlsbad, CA, USA) and total RNA was extracted following the manufacturer's protocol. Total RNA was cleaned and concentrated using an RNeasy Plus Mini Kit (Qiagen, Hilden, Germany). cDNA was synthesized using SuperScript III Reverse Transcriptase (Invitrogen) and Oligo(dT) primers according to the manufacturer's protocol. The resulting cDNA was used as template for all RT-PCR reactions. The full length ayRhp1 sequence was obtained following two rounds of RT-PCR using Phusion High Fidelity taq polymerase (New England Biolabs, Ipswitch, MA, USA) and NucleoSpin gel purification (Macherey-Nagel, Duren, Germany). The first round of RT-PCR used primers designed against untranslated regions of a predicted *Acropora digitifera* Rh mRNA (XP_015769291.1) (FWD primer 5'-CCACAATTCCGTC-3', REV primer 5'-GTCCGAGACATCTTGCATACC-3'). In the second 'nested' round of RT-PCR, primers included oligonucleotide overhangs for In-Fusion Cloning (Clontech, Mountain View, CA, USA) into a pCR2.1-TOPO vector (Invitrogen) digested with EcoR 1 and EcoR V restriction enzymes. All cloned RT-PCR products were sequenced by Retrogen, Inc. (San Diego, CA, USA). The full ayRhp1 sequence can be found on Genbank (MH025799).

Protein sequences for the phylogenetic analysis were sourced from (*74*) and Genbank via BLASTtn search. Sequences were aligned using MUSCLE (*79*) and a maximum likelihood tree with 500 bootstraps was inferred by RAxML using a PROTGAMMA model of rate heterogeneity and a GTR substitution model (*80*). Accession numbers of all Rh sequences used in this analysis can be found in the supporting information file (Table S1). Prediction of transmembrane helices was performed using TMHMM 2.0 (http://www.cbs.dtu.dk/services/TMHMM-2.0/) as per (*81*, *82*).

ayRhp1 Protein Expression and Antibody Validation in *A. yongei*

Using methods adapted from (*4*), *A. yongei* tissue was removed from the skeleton using an airbrush loaded with homogenization buffer. Homogenate was sonicated on ice for 4 x 10-sec bursts with 1 min rest in-between. The sonicated homogenate was then centrifuged (500 x g, 15 min, 4°C) to pellet down debris; the supernatant was kept on ice but not frozen. Sample

protein concentrations were determined using a Bradford Protein Assay (Bio-Rad, Hercules, CA, USA). 4x Laemmli buffer (Bio-Rad) and 10% β-mercaptoethanol were added to samples before heating at 90°C for 3 min. 22.5 µg protein and 4 µl of Precision Plus Dual Color Protein Standards (Bio-Rad) were loaded into a 10% polyacrylamide SDS-PAGE gel in a Mini-Trans Blot Cell (Bio-Rad) with running buffer (25 mM Tris, 190 mM glycine, 0.1% SDS). Electrophoresis was run for 100 min at 100 V (4°C).

Following electrophoresis, the gel was washed in distilled water for 5 min and equilibrated in Towbin buffer (25 mM Tris pH 8.3, 192 mM glycine, 20% (v/v) methanol) for 15 min. Proteins were transferred from the gel onto a PVDF membrane using a Mini Tans-Blot Cell (Bio-Rad) overnight in Towbin buffer (0.09 A, 4°C). PVDF membranes were washed in Tris-buffered Saline + 0.1% Tween detergent (TBS-T) for 15 min on a shaker at room temperature to remove excess transfer buffer prior to blocking. Membranes were then blocked with 5% powdered fat-free milk in TBS-T for 1 h on a shaker at room temperature.

Following blocking, membranes were incubated overnight on a shaker (4°C) with anti-ayRhp1 primary antibody (0.216 µg/ml), primary antibody with 400x excess peptide on a molar base ('pre-absorption control'), or pre-immune serum (0.216 µg/ml) diluted in blocking buffer. Membranes were then washed with 4 x 15-min TBS-T washes prior to incubation with secondary antibody (goat anti-rabbit-HRP diluted 1:10,000, Bio-Rad) for 1 h on a shaker at room temperature. Membranes were again washed with 4 x 15-min TBS-T washes and a final 15-min TBS wash prior to band development with an ECL Prime Western Blot Detection Kit (GE Healthcare, Chicago, IL, USA) and imaged using a Chemidoc Imaging system (Bio-Rad).

Confirmation of ayRhp1 Protein Expression in *Xenopus* Oocytes

Using methods adapted from (*83*), ayRhp1-expressing and control *Xenopus* oocytes were added to ice-cold homogenization buffer (250 mM sucrose, 1 mM EDTA, 30 mM TRIS in milliQ-water) spiked with protease inhibitor cocktail (MilliporeSigma, Burlington, MA, USA) at a ratio of 1 oocyte:50 µL. Oocytes were homogenized on ice by gentle pipetting and left for 20 mins at 4°C to solubilize membrane proteins. Homogenates were centrifuged (10,000 x g, 2 min, 4°C) to pellet yolk and debris; the lipid layers on top of the supernatants were removed and discarded. The supernatants were transferred to new tubes on ice and saved as crude homogenates. Sample protein concentrations were determined using a Bradford Protein Assay (Bio-Rad). 2x Laemmli buffer (Bio-Rad) and 10% β-mercaptoethanol was added to samples. Half of these homogenates were flash frozen in liquid nitrogen and returned to -80°C. The remaining crude homogenate was heated to 70°C for 15 min and 16.0 µg total protein was subjected to Western blotting as described in the Methods. The PDVF membranes were incubated overnight on a shaker (4°C) with anti-ayRhp1 antibodies (0.216 µg/ml), primary antibody with 400x excess peptide on a molar base ('pre-absorption control'), or anti-Tubulin mouse monoclonal antibody (4.7 ng/mL, 12G10 anti-alpha-tubulin, developed by J. Frankel and E.M. Nelsen, and obtained from the Developmental Studies Hybridoma Bank, created by the NICHD of the NIH and maintained at The University of Iowa, Department of Biology, Iowa City, IA 52242). PVDF membranes were processed as described in the Methods, using goat anti-rabbit-HRP or goat anti-mouse-HRP diluted 1:5,000 (Bio-Rad) as the secondary antibodies. The anti-ayRhp1 antibodies labeled a ~180 kDa band in ayRhp1-expressing oocytes which was

absent in control oocytes and in the pre-absorption control. This band corresponds to ayRhp1 trimers. (Fig. S6A).

The following day, the refrozen ayRhp1-expressing and control oocyte homogenates were thawed to promote dissociation of ayRhp1 trimers, mixed with 2x Laemmli buffer (Bio-Rad) and β-mercaptoethanol, heated to 70°C for 15 min, and subjected to Western blotting and imaging as described above. The anti-ayRhp1 antibodies labeled ~120 and ~60 kDa bands that are absent in the control oocytes and in the pre-absorption control. These bands correspond to ayRhp1 dimers and monomers, respectively. (Fig. S6B-C). In addition to confirming ayRhp1 expression in *Xenopus* oocytes, these results conform the specificity of the anti-ayRhp1 antibodies against ayRhp1.

Immunofluorescence

Following (*84*), *A. yongei* nubbins were fixed for immunohistochemistry by immersion in S22 buffer (450 mM NaCl, 10 mM KCl, 58 mM $MgCl_2$, 10 mM $CaCl_2$, 100 mM Hepes, pH 7.80) supplemented with 4% paraformaldehyde overnight on a rocking platform at 4°C. Nubbins were then transferred to calcium-free S22 buffer supplemented with 0.5 M EDTA to decalcify the skeleton and with 0.5% paraformaldehyde to preserve tissue fixation; this decalcification buffer was changed daily for 2 weeks. Once decalcified, nubbins were dehydrated (50% ethanol for 5 h, 70% ethanol overnight, 95% ethanol for 20 min, 100% ethanol 3 x 20 min, SafeClear for 3 x 20 min), embedded in paraffin wax (3 x 30 min) and allowed to solidify for 48 h before microtome sectioning onto glass slides. *A. yongei* tissue sections were deparaffinized and serially rehydrated in SafeClear for 3 x 10 min, 100% ethanol for 10 min, 95% ethanol for 10 min, 70% ethanol for 10 min, and PBS with 0.2% (v/v) Triton-X-100 (PBS-TX) for 10 min.

Using methods adapted from (*84*, *49*), isolated *A. yongei* cells were prepared by submerging a nubbin in 0.2 µm filtered seawater and brushed with a toothbrush for 1 min. Cells were collected via centrifugation (3,000 x g, 4 minutes, 4°C) and fixed by resuspension in S22 buffer with 4% paraformaldehyde for 15 min on ice. Fixative was removed via centrifugation (3,000 x g, 4 minutes, 4°C) and cells were resuspended in ~500µL of S22 buffer. Cells were then pipetted onto glass microscope slide and allowed to air dry at 4°C for no longer than 1 h before proceeding to immunolabeling.

Tissue sections and isolated cells were blocked for 1 h at room temperature in blocking buffer (4 ml PBS-TX, 80 µl normal goat serum, 0.8 µl keyhole limpet hemocyanin solution), followed by overnight incubation (4°C) with anti-ayRhp1 antibodies (2.16 µg/ml), anti-ayRhp1 antibodies pre-absorbed with excess peptide (8.64 µg/ml) or pre-immune serum (2.16 µg/ml) (all in blocking buffer) (Fig. S4D). Slides were washed in PBS-TX to remove unbound anti-ayRhp1 antibodies (3 x 5 min). Secondary antibodies (goat anti-rabbit-Alexa Fluor555, 4 µg/ml in blocking buffer; Invitrogen) were then added for 1 h at room temperature followed by DAPI DNA Stain (1 µg/ml; Invitrogen) for 5 min at room temperature. Slides were again washed PBS-TX to remove unbound secondary antibody (3 x 5 min) and samples were imaged using a fluorescence microscope (Zeiss AxioObserver, Carl Zeiss AG, Oberkochen, Germany).

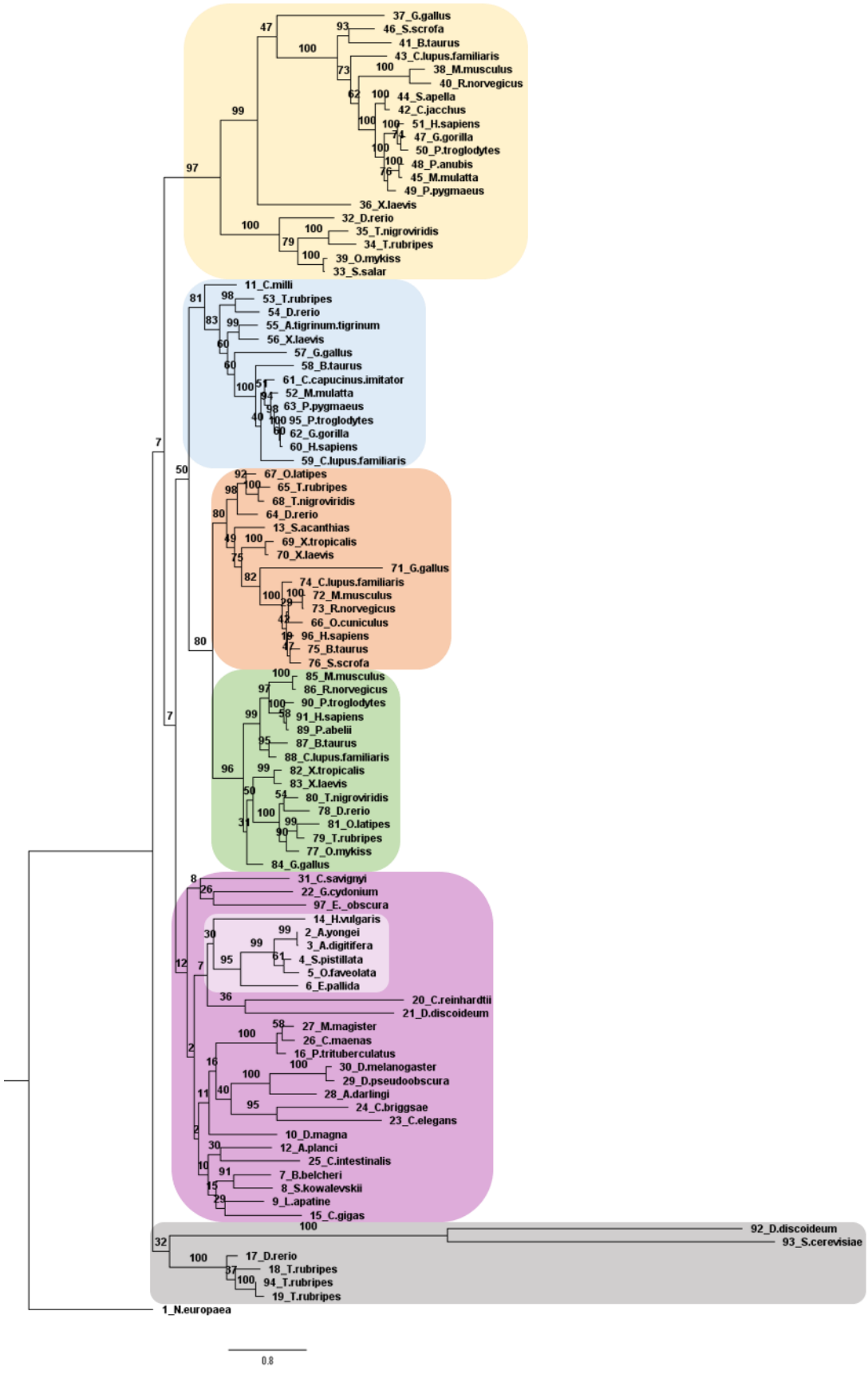
37_G.gallus
46_S.scrofa
41_B.taurus
43_C.lupus.familiaris
38_M.musculus
40_R.norvegicus
44_S.apella
42_C.jacchus
51_H.sapiens
47_G.gorilla
50_P.troglodytes
48_P.anubis
45_M.mulatta
49_P.pygmaeus
36_X.laevis
32_D.rerio
35_T.nigroviridis
34_T.rubripes
39_O.mykiss
33_S.salar
11_C.milli
53_T.rubripes
54_D.rerio
55_A.tigrinum.tigrinum
56_X.laevis
57_G.gallus
58_B.taurus
61_C.capucinus.imitator
52_M.mulatta
63_P.pygmaeus
95_P.troglodytes
62_G.gorilla
60_H.sapiens
59_C.lupus.familiaris
67_O.latipes
65_T.rubripes
68_T.nigroviridis
64_D.rerio
13_S.acanthias
69_X.tropicalis
70_X.laevis
71_G.gallus
74_C.lupus.familiaris
72_M.musculus
73_R.norvegicus
66_O.cuniculus
96_H.sapiens
75_B.taurus
76_S.scrofa
85_M.musculus
86_R.norvegicus
90_P.troglodytes
91_H.sapiens
89_P.abelii
87_B.taurus
88_C.lupus.familiaris
82_X.tropicalis
83_X.laevis
80_T.nigroviridis
78_D.rerio
81_O.latipes
79_T.rubripes
77_O.mykiss
84_G.gallus
31_C.savignyi
22_G.cydonium
97_E._obscura
14_H.vulgaris
2_A.yongei
3_A.digitifera
4_S.pistillata
5_O.faveolata
6_E.pallida
20_C.reinhardtii
21_D.discoideum
27_M.magister
26_C.maenas
16_P.trituberculatus
30_D.melanogaster
29_D.pseudoobscura
28_A.darlingi
24_C.briggsae
23_C.elegans
10_D.magna
12_A.planci
25_C.intestinalis
7_B.belcheri
8_S.kowalevskii
9_L.apatine
15_C.gigas
92_D.discoideum
93_S.cerevisiae
17_D.rerio
18_T.rubripes
94_T.rubripes
19_T.rubripes
1_N.europaea
0.8

Supplementary Figure 1: Maximum likelihood tree of the *Acropora yongei* Rhesus protein (ayRhp1) in relation to invertebrate and vertebrate Rh proteins. Rh family subgroups are denoted by color: Rh30 (yellow), Rhag (blue), Rhbg (orange), Rhcg (green), Rhp1 (light and dark purple), and Rhp2 (grey) as per (*2*). Cnidarian Rh proteins are highlighted within the Rhp1 subgroup (light purple). Amino acid sequences were aligned using MUSCLE and a maximum likelihood tree was generated using RAxML (500 bootstraps, PROTGAMMA model of rate heterogeneity, GTR substitution model). Sequences and the outgroup (*Nitrosoma europaea* Rh) are sourced from (*2*) with additional sequences identified by NCBI BLAST search. Sequence accession numbers are provided in Supplementary Table 1.

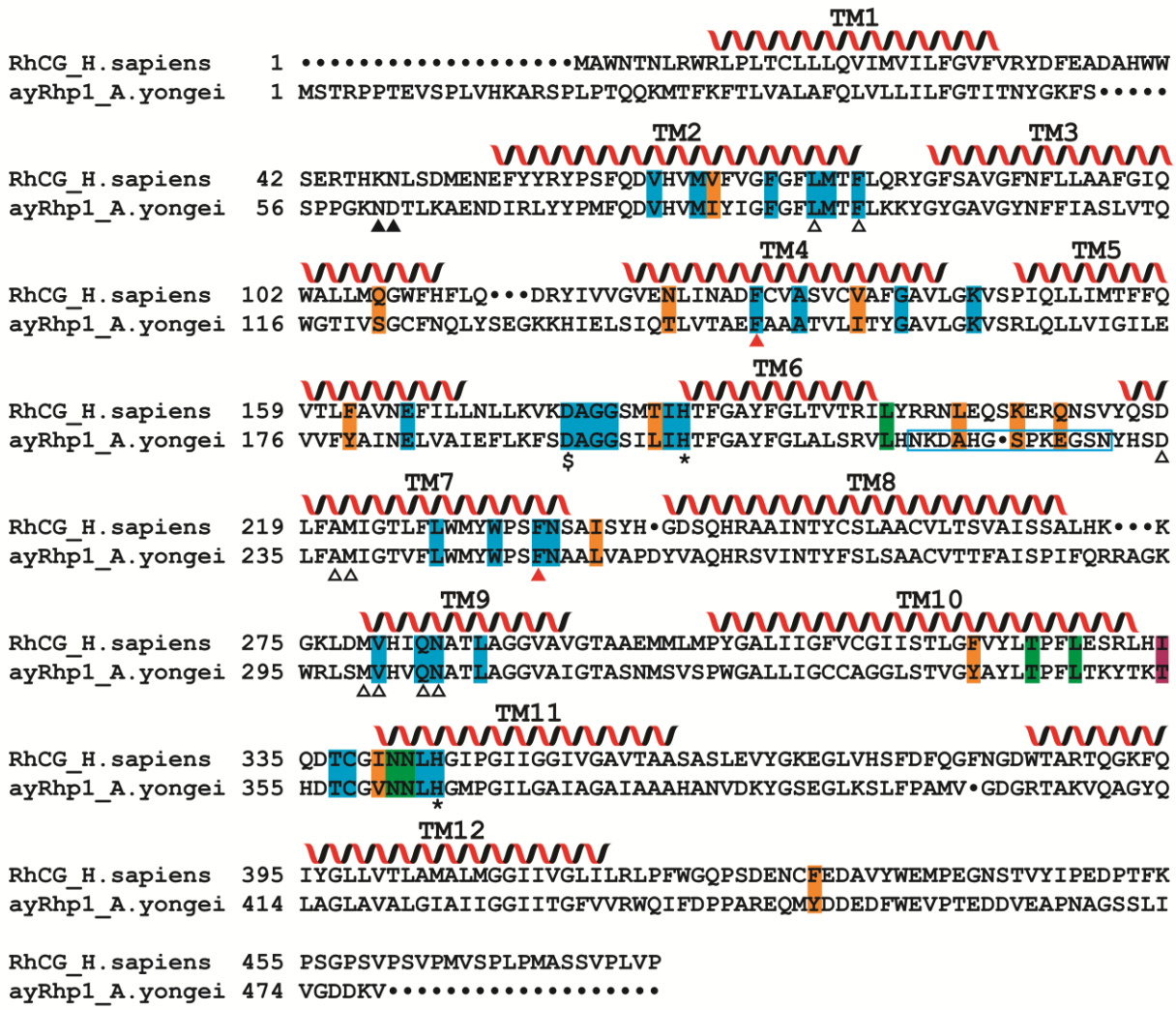

Supplementary Figure 2: Alignment of *Acropora yongei* Rhesus protein (ayRhp1) with *Homo sapiens* RhCG (NP_001307970.1). Conserved (blue) and mismatched (orange) hydrophobic channel-lining residues, conserved (green) and mismatched (magenta) cytosolic shunt residues, N-glycan site (black filled triangles), CO_2 binding pocket (black outlined triangles) as discussed in (*35*), Phe-gate (red filled triangles), twin-Histidines (*), and the highly-conserved aspartate residues ($) as discussed in (*20*, *34*) are marked. Gaps in sequences are denoted by black dots. The 12 transmembrane helices (TM), as predicted by TMHMM 2.0 (*5*, *6*), for RhCG (*20*) and ayRhp1 are labeled with spirals.

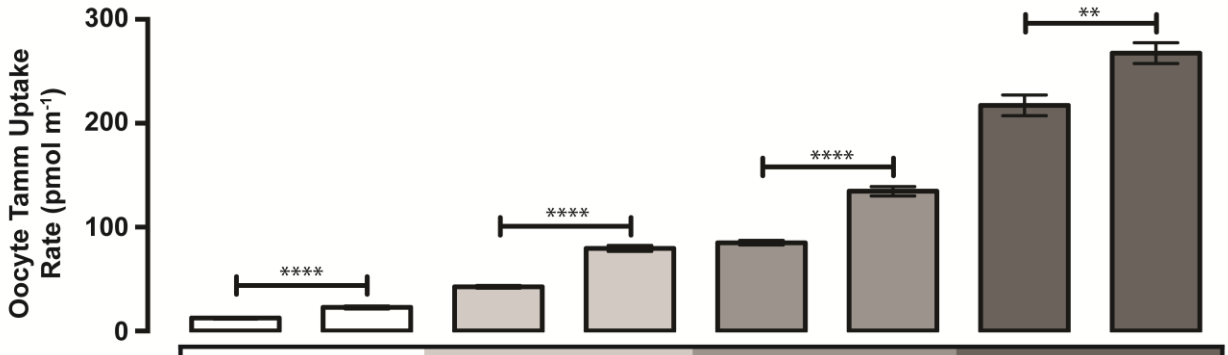

	Control	ayRhp1	Control	ayRhp1	Control	ayRhp1	Control	ayRhp1
pH	6.5	6.5	7.5	7.5	8.5	8.5	7.5	7.5
Tamm (µM)	1,000	1,000	1,000	1,000	1,000	1,000	10,000	10,000
$[NH_3]$ (µM)	1.8	1.8	17.4	17.4	150.5	150.5	174.0	174.0
$[NH_4^+]$ (µM)	998.2	998.2	982.6	982.6	849.5	849.5	9826	9826

Supplementary Figure 3: Effect of $[NH_3]$ on total ammonium (Tamm) uptake rate in *Xenopus* oocytes expressing *Acropora yongei* Rhesus protein (ayRhp1). Data shows mean ± S.E.M. of 6-14 oocytes; * denote significant differences (unpaired t-test; ***p<0.01; ****p<0.001*).

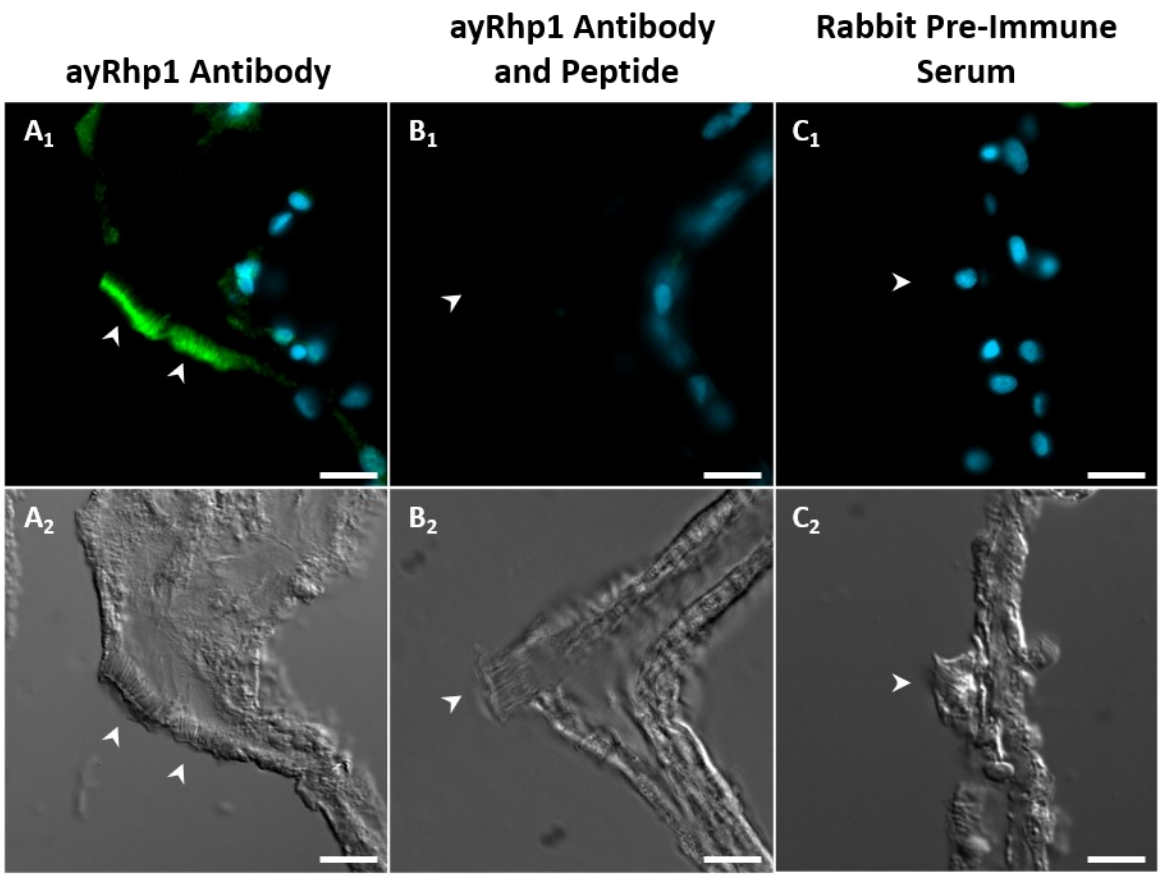

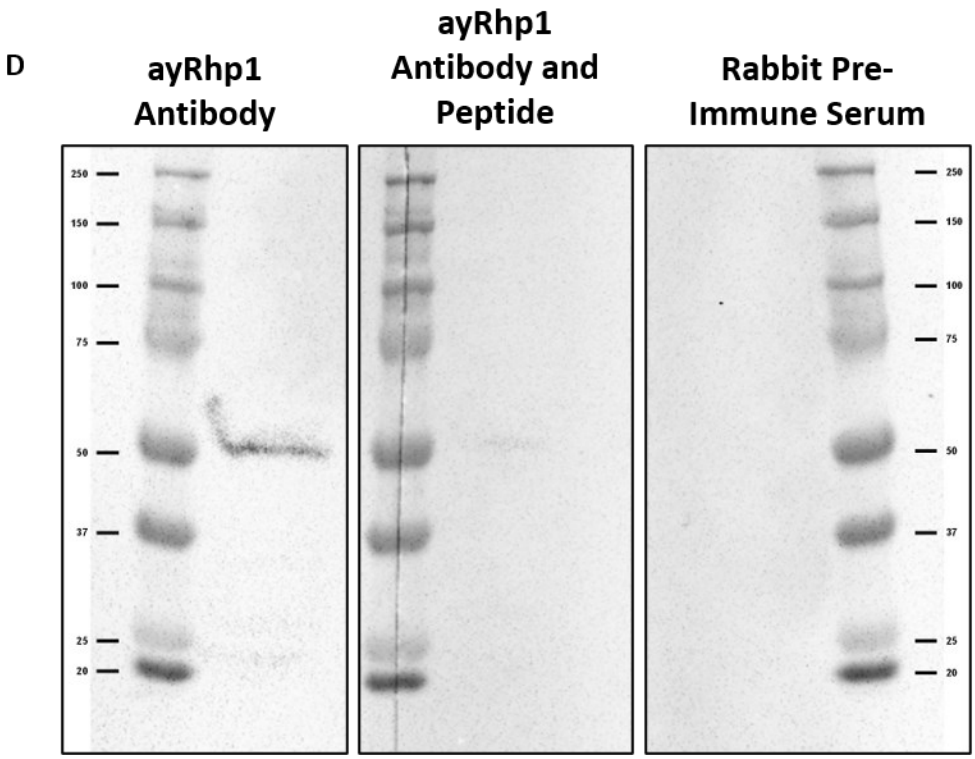

Supplementary Figure 4: Immunohistochemistry and Western Blot validation of the custom anti-*Acropora yongei* Rhesus protein (ayRhp1) antibody. Tissue sections were incubated with

anti-ayRhp1 primary antibody, primary antibody with excess peptide, or pre-immune serum at an equal concentration to primary antibody alone. Anti-ayRhp1 antibody signal dissipates with peptide incubation and is absent in pre-immune serum incubations. **(A_1-C_1)** Desmocytes in tissue sections; desmocytes are the most brightly-labeled cell type in *A. yongei* tissues. **(A_2-C_2)** corresponding brightfield differential interference contrast images. Nuclei are shown in blue, ayRhp1 in red. White arrowheads mark corresponding locations in epifluorescence and brightfield images. Scale bars = 10 μm. **(D)** Western Blot validation of the custom ayRhp1 antibody. Membranes were labeled with anti-ayRhp1 primary antibody, primary antibody with excess peptide, or pre-immune serum at an equal concentration to primary antibody alone.

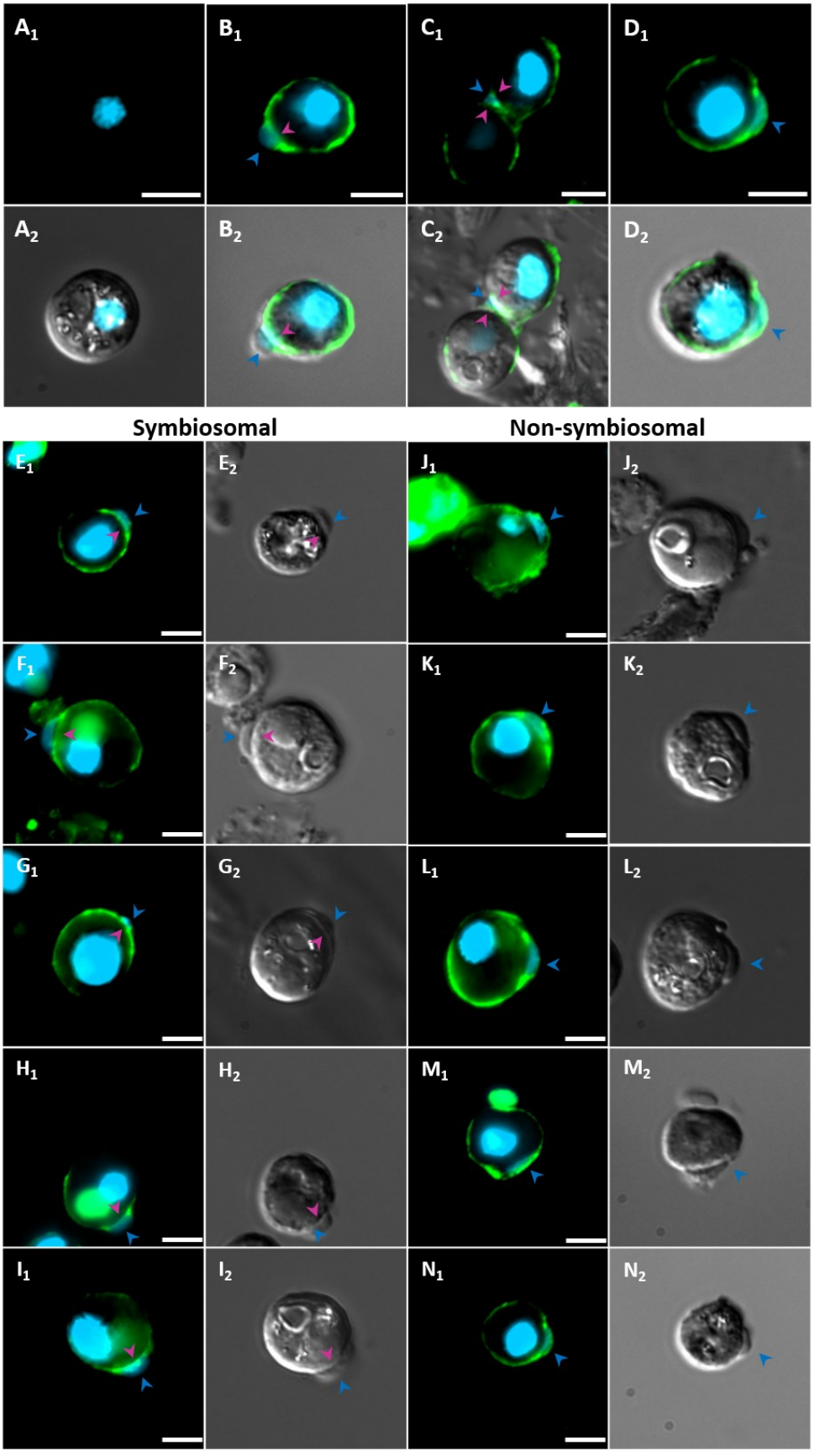
A1
B1
C1
D1
A2
B2
C2
D2
Symbiosomal
Non-symbiosomal
E1
E2
J1
J2
F1
F2
K1
K2
G1
G2
L1
L2
H1
H2
M1
M2
I1
I2
N1
N2

Supplementary Figure 5: Epifluorescence immunolocalization of *Acropora yongei* Rhesus protein (ayRhp1) in isolated alga-hosting gastrodermal cells. (**A_1**) Algal symbiont isolated from its host cell. (**B_1**) A coral host cell with ayRhp1 on the symbiosome membrane. (**C_1**) A coral host cell containing two algal symbionts with ayRhp1 on both symbiosome membranes. (**D_1**) A coral host cell with ayRhp1 on the exterior and sides of the host nucleus. **(E-N)** Further representative epifluorescence images of ayRhp1 in isolated alga-hosting gastrodermal cells. (**B_1, D_1, E_1-I_1**) Cells displaying ayRhp1 in the symbiosome membrane; notice the separation of host and algal nuclei by ayRhp1. (**D_1, F1-N_1**) Cells displaying non-symbiosomal ayRhp1; notice ayRhp1 signal exterior to the host nucleus and absent between the host and algal nuclei. (**A_2-N_2**) Corresponding images without brightfield differential interference contrast. Blue arrowheads mark nuclei of host cells; violet arrowheads mark ayRhp1 symbiosome localization. Nuclei are shown in blue and ayRhp1 in green. Scale bars = 5 μm.

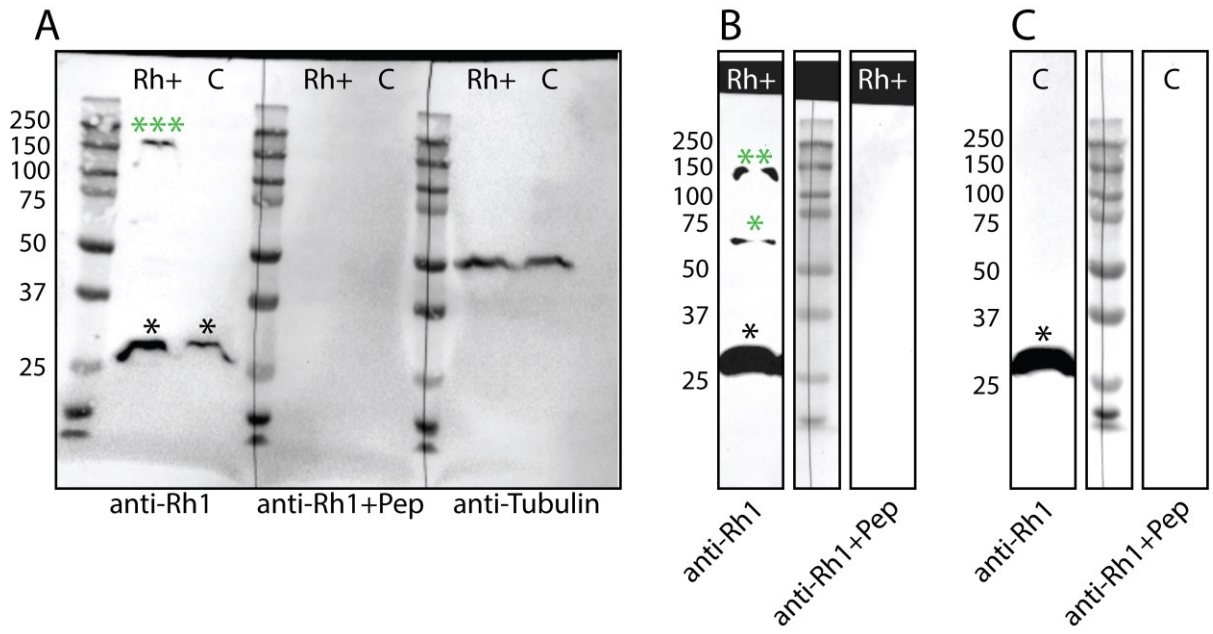

Supplementary Figure 6: Western Blot validation of ayRhp1 expression in *Xenopus* oocytes. (**A**) Western Blot of once-thawed ayRhp1-expressing (Rh+) and control (C) oocytes, which were homogenized and heated at 70°C for 15 min before loading into the gels. PVDF membranes were incubated with anti-ayRhp1 antibodies, anti-ayRhp1 antibodies pre-incubated with excess peptide (pre-absorption control), or anti-Tubulin antibody (12G10 anti-alpha-tubulin, developed by J. Frankel and E.M. Nelsen, and obtained from the Developmental Studies Hybridoma Bank, created by the NICHD of the NIH and maintained at The University of Iowa, Department of Biology, Iowa City, IA 52242).The anti-ayRhp1 antibodies labeled a ~180 kDa band in Rh+ oocytes which was absent in C oocytes (marked with three green asterisks) and in the pre-absorption control. This band corresponds to ayRhp1 trimers. The antibodies additionally labeled a ~29 kDa band in both Rh+ and C oocytes (marked with a black asterisk) which was not present in the pre-absoprtion control; this band represents off-target recognition of *Xenopus* protein(s). The anti-tubulin antibody labeled a ~50 kDa protein in both treatments demonstrating equivalent protein concentration in Rh+ and C samples. (**B, C**) Western Blots of rethawed Rh+ (**B**) and C (**C**) oocyte homogenates which were heated at 70°C for 15 min before loading into the gels. The anti-ayRhp1 antibodies labeled a ~120 kDa band (marked with two red asterisks) and a ~60 kDa band (marked with one red asterisk) that are absent in the C oocytes and in the pre-absorption control. These bands correspond to ayRhp1 dimers and monomers, respectively. The ~29 kDa band is still present in the rethawed homogenates.

Supplementary Table 1: NCBI accession numbers for sequences used in phylogenetic analysis (Fig. S1).

ID	Accession Number	Organism
1	AY377923.1	Nitrosomonas europaea
2	MH025799	Acropora yongei
3	XP_015769291.1	Acropora digitifera
4	XP_022795556.1	Stylophora pistillata
5	XP_020600999.1	Orbicella faveolata
6	KXJ18310.1	Exaiptasia pallida
7	XP_019645061.1	Branchiostoma belcheri
8	XP_006824549.1	Saccoglossus kowalevskii
9	XP_013381459.1	Lingula anatine
10	KZS19566.1	Daphnia magna
11	AFK10779.1	Callorhinchus milii
12	XP_022107421.1	Acanthaster planci
13	AJF44128.1	Squalus acanthias
14	XP_002167946.3	Hydra vulgaris
15	EKC21768.1	Crassostrea gigas
16	AHY27545.2	Portunus trituberculatus
17	NP_571622.1	Danio rerio
18	NP_001027816.1	Takifugu rubripes
19	NP_001027817.1	Takifugu rubripes
20	XP_001695464.1	Chlamydomonas reinhardtii
21	XP_639042.1	Dictyostelium discoideum
22	CAA73029.1	Geodia cydonium
23	AAF97864.1	Caenorhabditis elegans
24	XP_002636925.1	Caenorhabditis briggsae
25	NP_001027959.1	Ciona intestinalis
26	AAK50057.2	Carcinus maenas
27	AEA41159.1	Metacarcinus magister
28	ETN62951.1	Anopheles darlingi
29	AAV40852.1	Drosophila pseudoobscura
30	NP_001261434.1	Drosophila melanogaster
31	AAY41910.1	Ciona savignyi
32	NP_001019990.1	Danio rerio
33	NP_001117044.1	Salmo salar
34	NP_001027935.1	Takifugu rubripes
35	AAY41905.1	Tetraodon nigroviridis
36	NP_001084416.1	Xenopus laevis
37	NP_989798.1	Gallus gallus
38	AAC25123.1	Mus musculus
39	AAP87367.1	Oncorhynchus mykiss

40	NP_071950.1	Rattus norvegicus
41	NP_777137.1	Bos taurus
42	AAF22442.1	Callithrix jacchus
43	NP_001041501.1	Canis lupus familiaris
44	AAF22501.1	Sapajus apella
45	NP_001028136.3	Macaca mulatta
46	NP_999543.1	Sus scrofa
47	NP_001266526.1	Gorilla gorilla
48	XP_003891396.1	Papio anubis
49	AAC94962.1	Pongo pygmaeus
50	Q28813.2	Pan troglodytes
51	P18577.2	Homo sapiens
52	NP_001027987.1	Macaca mulatta
53	NP_001032956.1	Takifugu rubripes
54	NP_998010.1	Danio rerio
55	AAV28818.1	Ambystoma tigrinum tigrinum
56	XP_018121493.1	Xenopus laevis
57	NP_989795.1	Gallus gallus
58	NP_776596.1	Bos taurus
59	NP_001104238.1	Canis lupus familiaris
60	AHY04440.1	Homo sapiens
61	XP_017354151.1	Cebus capucinus imitator
62	NP_001266499.1	Gorilla gorilla
63	AAG00305.1	Pongo pygmaeus
64	NP_956365.2	Danio rerio
65	NP_001027818.1	Takifugu rubripes
66	NP_001075605.1	Oryctolagus cuniculus
67	NP_001098561.1	Oryzias latipes
68	Q3BBX8.1	Tetraodon nigroviridis
69	NP_001011175.1	Xenopus tropicalis
70	Q69D48.1	Xenopus laevis
71	AAN34362.1	Gallus gallus
72	AAF19371.1	Mus musculus
73	NP_898877.1	Rattus norvegicus
74	NP_001003017.2	Canis lupus familiaris
75	NP_777148.1	Bos taurus
76	NP_999161.1	Sus scrofa
77	NP_001117995.1	Oncorhynchus mykiss
78	AAM90586.1	Danio rerio
79	NP_001027934.1	Takifugu rubripes
80	Q3BBX7.1	Tetraodon nigroviridis
81	NP_001116374.1	Oryzias latipes
82	XP_012814245.1	Xenopus tropicalis

83	Q5U4V1.1	Xenopus laevis
84	NP_001004370.1	Gallus gallus
85	AAF19373.1	Mus musculus
86	NP_898876.1	Rattus norvegicus
87	NP_776597.1	Bos taurus
88	NP_001041487.1	Canis lupus familiaris
89	XP_002825848.1	Pongo abelii
90	XP_016782540.1	Pan troglodytes
91	NP_057405.1	Homo sapiens
92	BAB39709.1	Dictyostelium discoideum
93	X77608.1	Saccharomyces cerevisiae
94	AAU81656.1	Takifugu rubripes
95	NP_001009033.1	Pan troglodytes
96	AF193807.1	Homo sapiens
97	AJO26542.1	Erpobdella obscura

SI Files

Data S1

Cell count data used for determining diel ayRhp1 localization in coral host cells.

REFERENCES AND NOTES

1. M. J. H. van Oppen, M. Medina, Coral evolutionary responses to microbial symbioses. *Philos. Trans. R. Soc. Lond. B Biol. Sci.* **375**, 20190591 (2020).

2. Y. Tanaka, A. Suzuki, K. Sakai, The stoichiometry of coral-dinoflagellate symbiosis: Carbon and nitrogen cycles are balanced in the recycling and double translocation system. *ISME J.* **12**, 860–868 (2018).

3. B. L. Tang, Thoughts on a very acidic symbiosome. *Front. Microbiol.* **6**, 816 (2015).

4. K. L. Barott, A. A. Venn, S. O. Perez, S. Tambutté, M. Tresguerres, Coral host cells acidify symbiotic algal microenvironment to promote photosynthesis. *Proc. Natl. Acad. Sci. U.S.A.* **112**, 607–612 (2015).

5. O. Rahav, Z. Dubinsky, Y. Achituv, P. G. Falkowski, Ammonium metabolism in the zooxanthellate coral, *Stylophora pistillata*. *Proc. R. Soc. Lond. B.* **236**, 325–337 (1989).

6. P. A. Wright, Nitrogen excretion: Three end products, many physiological roles. *J. Exp. Biol.* **198**, 273–281 (1995).

7. A. M. Szmant, L. M. Ferrer, L. M. FitzGerald, Nitrogen excretion and O:N ratios in reef corals: Evidence for conservation of nitrogen. *Mar. Biol.* **104**, 119–127 (1990).

8. G. Cui, Y. J. Liew, Y. Li, N. Kharbatia, N. I. Zahran, A. H. Emwas, V. M. Eguiluz, M. Aranda, Host-dependent nitrogen recycling as a mechanism of symbiont control in *Aiptasia*. **15**, e1008189 (2019).

9. C. Kopp, M. Pernice, I. Domart-Coulon, C. Djediat, J. E. Spangenberg, D. T. L. Alexander, M. Hignette, T. Meziane, A. Meibom, Highly dynamic cellular-level response of symbiotic coral to a sudden increase in environmental nitrogen. *mBio* **4**, e00052-13 (2013).

10. C. D'Elia, S. Domotor, K. Webb, Nutrient uptake kinetics of freshly isolated zooxanthellae*. *Mar. Biol.* **167**, 157–167 (1983).

11. M. Pernice, A. Meibom, A. Van Den Heuvel, C. Kopp, I. Domart-Coulon, O. Hoegh-Guldberg, S. Dove, A single-cell view of ammonium assimilation in coral-dinoflagellate symbiosis. *ISME J.* **6**, 1314–1324 (2012).

12. T. A. V. Rees, Are symbiotic algae nutrient deficient? *Proc. R. Soc. B Biol. Sci.* **243**, 227–233 (1991).

13. T. Krueger, N. Horwitz, J. Bodin, M. E. Giovani, S. Escrig, M. Fine, A. Meibom, Intracellular competition for nitrogen controls dinoflagellate population density in corals. *Proc. Biol. Sci.* **287**, 20200049 (2020).

14. A. E. Sproles, N. L. Kirk, S. A. Kitchen, C. A. Oakley, A. R. Grossman, V. M. Weis, S. K. Davy, Phylogenetic characterization of transporter proteins in the cnidarian-dinoflagellate symbiosis. *Mol. Phylogenet. Evol.* **120**, 307–320 (2018).

15. K. L. Barott, M. E. Barron, M. Tresguerres, Identification of a molecular pH sensor in coral. *Proc. R. Soc. B* **284**, 20171769 (2017).

16. I. D. Weiner, J. W. Verlander, Ammonia transporters and their role in acid-base balance. *Physiol. Rev.* **97**, 465–494 (2017).

17. I. S. Wallace, W.-G. Choi, D. M. Roberts, The structure, function and regulation of the nodulin 26-like intrinsic protein family of plant aquaglyceroporins. *Biochim. Biophys. Acta* **1758**, 1165–1175 (2006).

18. C. M. Niemietz, S. D. Tyerman, Channel-mediated permeation of ammonia gas through the peribacteroid membrane of soybean nodules. *FEBS Lett.* **465**, 110–114 (2000).

19. R. R. Geyer, M. D. Parker, A. M. Toye, W. F. Boron, R. Musa-Aziz, Relative CO_2/NH_3 permeabilities of human RhAG, RhBG and RhCG. *J. Membr. Biol.* **246**, 915–926 (2013).

20. F. Gruswitz, S. Chaudhary, J. D. Ho, A. Schlessinger, B. Pezeshki, C.-M. Ho, A. Sali, C. M. Westhoff, R. M. Stroud, Function of human Rh based on structure of RhCG at 2.1 A. *Proc. Natl. Acad. Sci. U.S.A.* **107**, 9638–9643 (2010).

21. S. Baday, E. A. Orabi, S. Wang, G. Lamoureux, S. Bernèche, Mechanism of NH_4^+ recruitment and NH_3 transport in Rh proteins. *Structure* **23**, 1550–1557 (2015).

22. E. M. Lehnert, M. E. Mouchka, M. S. Burriesci, N. D. Gallo, J. A. Schwarz, J. R. Pringle, Extensive differences in gene expression between symbiotic and aposymbiotic cnidarians. *G3* **4**, 277–295 (2014).

23. Y. Ishii, S. Maruyama, H. Takahashi, Y. Aihara, T. Yamaguchi, K. Yamaguchi, S. Shigenobu, M. Kawata, N. Ueno, J. Minagawa, Global shifts in gene expression profiles accompanied with environmental changes in cnidarian-dinoflagellate endosymbiosis. *G3* **9**, 2337–2347 (2019).

24. P. Ganot, A. Moya, V. Magnone, D. Allemand, P. Furla, C. Sabourault, Adaptations to endosymbiosis in a Cnidarian-Dinoflagellate association: Differential gene expression and specific gene duplications. *PLOS Genet.* **7**, e1002187 (2011).

25. M. Hu, X. Zheng, C.-M. Fan, Y. Zheng, Lineage dynamics of the endosymbiotic cell type in the soft coral *Xenia*. *Nature* **582**, 534–538 (2020).

26. D. Weihrauch, M. O'Donnell, *Acid-Base Balance and Nitrogen Excretion in Invertebrates* (Springer International Publishing, 2017); http://link.springer.com/10.1007/978-3-319-39617-0.

27. M. Benghezal, D. Gotthardt, S. Cornillon, P. Cosson, Localization of the Rh50-like protein to the contractile vacuole in *Dictyostelium*. *Immunogenetics* **52**, 284–288 (2001).

28. K. H. Han, K. Mekala, V. Babida, H. Y. Kim, M. E. Handlogten, J. W. Verlander, I. D. Weiner, Expression of the gas-transporting proteins, Rh B glycoprotein and Rh C glycoprotein, in the murine lung. *Am. J. Physiol. Lung Cell. Mol. Physiol.* **297**, L153–L163 (2009).

29. S. F. Perry, M. H. Braun, M. Noland, J. Dawdy, P. J. Walsh, Do zebrafish Rh proteins act as dual ammonia-CO2 channels? *J. Exp. Zool. A Ecol. Genet. Physiol.* **313**, 618–621 (2010).

30. V. Endeward, J. P. Cartron, P. Ripoche, G. Gros, RhAG protein of the Rhesus complex is a CO2 channel in the human red cell membrane. *FASEB J.* **22**, 64–73 (2008).

31. C. M. Nawata, C. M. Wood, M. J. O'Donnell, Functional characterization of Rhesus glycoproteins from an ammoniotelic teleost, the rainbow trout, using oocyte expression and SIET analysis. *J. Exp. Biol.* **213**, 1049–1059 (2010).

32. X.-D. Li, D. Lupo, L. Zheng, F. Winkler, Structural and functional insights into the AmtB/Mep/Rh protein family. *Transfus. Clin. Biol.* **13**, 65–69 (2006).

33. J. Stolarski, M. V. Kitahara, D. J. Miller, S. D. Cairns, M. Mazur, A. Meibom, The ancient evolutionary origins of Scleractinia revealed by azooxanthellate corals. *BMC Evol. Biol.* **11**, 316 (2011).

34. A. M. Marini, M. Boeckstaens, F. Benjelloun, B. Chérif-Zahar, B. André, Structural involvement in substrate recognition of an essential aspartate residue conserved in Mep/Amt and Rh-type ammonium transporters. *Curr. Genet.* **49**, 364–374 (2006).

35. X. Li, S. Jayachandran, H.-H. H. T. Nguyen, M. K. Chan, Structure of the *Nitrosomonas europaea* Rh protein. *Proc. Natl. Acad. Sci. U.S.A.* **104**, 19279–19284 (2007).

36. D. J. Lee, M. Gutbrod, F. M. Ferreras, P. G. D. Matthews, Changes in hemolymph total CO_2 content during the water-to-air respiratory transition of amphibiotic dragonflies. *J. Exp. Biol.* **221**, jeb181438 (2018).

37. S. Sasaki, K. Ishibashi, T. Nagai, F. Marumo, Regulation mechanisms of intracellular pH of *Xenopus laevis* oocyte. *Biochim. Biophys. Acta* **1137**, 45–51 (1992).

38. J. Thomsen, N. Himmerkus, N. Holland, F. J. Sartoris, M. Bleich, M. Tresguerres, Ammonia excretion in mytilid mussels is facilitated by ciliary beating. *J. Exp. Biol.* **219**, 2300–2310 (2016).

39. P. A. Wright, C. M. Wood, A new paradigm for ammonia excretion in aquatic animals: Role of Rhesus (Rh) glycoproteins. *J. Exp. Biol.* **212**, 2303–2312 (2009).

40. D. Thiel, M. Hugenschutt, H. Meyer, A. Paululat, A. R. Quijada-Rodriguez, G. Purschke, D. Weihrauch, Ammonia excretion in the marine polychaete Eurythoe complanata (Annelida). *J. Exp. Biol.* **220**, 425–436 (2017).

41. J. G. Tidball, Fine structural aspects of anthozoan desmocyte development (Phylum Cnidaria). *Tissue Cell* **14**, 85–96 (1982).

42. L. Muscatine, E. Tambutte, D. Allemand, Morphology of coral desmocytes, cells that anchor the calicoblastic epithelium to the skeleton. *Coral Reefs* **16**, 205–213 (1997).

43. J. W. Campbell, K. V. Speeg, Ammonia and biological deposition of calcium carbonate. *Nature* **224**, 725–726 (1969).

44. R. A. Loest, Ammonia-forming enzymes and calcium-carbonate deposition in terrestrial pulmonates. *Physiol. Zool.* **52**, 470–483 (1979).

45. C. J. Crossland, D. J. Barnes, The role of metabolic nitrogen in coral calcification. *Mar. Biol.* **28**, 325–332 (1974).

46. W. J. Cai, Y. Ma, B. M. Hopkinson, A. G. Grottoli, M. E. Warner, Q. Ding, X. Hu, X. Yuan, V. Schoepf, H. Xu, C. Han, T. F. Melman, K. D. Hoadley, D. T. Pettay, Y. Matsui, J. H. Baumann, S. Levas, Y. Ying, Y. Wang, Microelectrode characterization of coral daytime interior pH and carbonate chemistry. *Nat. Commun.* **7**, 11144 (2016).

47. N. Allison, I. Cohen, A. A. Finch, J. Erez, A. W. Tudhope, Corals concentrate dissolved inorganic carbon to facilitate calcification. *Nat. Commun.* **5**, 5741 (2014).

48. J. H. Kaplan, Biochemistry of Na,K-ATPase. *Annu. Rev. Biochem.* **71**, 511–535 (2002).

49. A. A. Venn, E. Tambutté, S. Lotto, D. Zoccola, D. Allemand, S. Tambutté, Imaging intracellular pH in a reef coral and symbiotic anemone. *Proc. Natl. Acad. Sci. U.S.A.* **106**, 16574–9 (2009).

50. M. Y. Hu, Y. J. Guh, M. Stumpp, J. R. Lee, R. D. Chen, P. H. Sung, Y. C. Chen, P. P. Hwang, Y. C. Tseng, Branchial NH_4^+-dependent acid-base transport mechanisms and energy metabolism of squid (*Sepioteuthis lessoniana*) affected by seawater acidification. *Front. Zool.* **11**, (2014), doi:10.1186/s12983-014-0055-z.

51. A. Bertucci, A. Moya, S. Tambutté, D. Allemand, C. T. Supuran, D. Zoccola, Carbonic anhydrases in anthozoan corals - a review. *Bioorg. Med. Chem.* **21**, 1437–1450 (2013).

52. I. D. Weiner, J. W. Verlander, Renal ammonia metabolism and transport. *Compr. Physiol.* **3**, 201–220 (2013).

53. R. Grover, J.-F. Maguer, S. Reynaud-vaganay, C. Ferrier-Pagès, Uptake of ammonium by the scleractinian coral *Stylophora pistillata*: Effect of feeding, light, and ammonium concentrations. *Limnol. Oceanogr.* **47**, 782–790 (2002).

54. E. Beraud, F. Gevaert, C. Rottier, C. Ferrier-Pages, The response of the scleractinian coral Turbinaria reniformis to thermal stress depends on the nitrogen status of the coral holobiont. *J. Exp. Biol.* **216**, 2665–2674 (2013).

55. N. Rosic, P. Kaniewska, C.-K. Chan, E. Y. Ling, D. Edwards, S. Dove, O. Hoegh-Guldberg, Early transcriptional changes in the reef-building coral Acropora aspera in response to thermal and nutrient stress. *BMC Genomics* **15**, 1052 (2014).

56. S. Agostini, Y. Suzuki, T. Higuchi, B. E. Casareto, K. Yoshinaga, Y. Nakano, H. Fujimura, Biological and chemical characteristics of the coral gastric cavity. *Coral Reefs* **31**, 147–156 (2012).

57. P. Furla, I. Galgani, I. Durand, D. Allemand, Sources and mechanisms of inorganic carbon transport for coral calcification and photosynthesis. *J. Exp. Biol.* **203**, 3445–3457 (2000).

58. D. Yellowlees, T. A. V. Rees, W. Leggat, Metabolic interactions between algal symbionts and invertebrate hosts. *Plant. Cell Environ.* **31**, 679–694 (2008).

59. C. A. Oakley, M. F. Ameismeier, L. Peng, V. M. Weis, A. R. Grossman, S. K. Davy, Symbiosis induces widespread changes in the proteome of the model cnidarian *Aiptasia*. *Cell. Microbiol.* **18**, 1009–1023 (2016).

60. D. Yellowlees, T. Rees, W. Fitt, Effect of ammonium-supplemented seawater on glutamine synthetase and glutamate dehydrogenase activities in host tissue and zooxanthellae of Pocillopora damicornis and on ammonium uptake rates of the zooxanthellae. *Pacific Sci.* **48**, 291–295 (1994).

61. J. Tang, X. Ni, J. Wen, L. Wang, J. Luo, Z. Zhou, Increased ammonium assimilation activity in the scleractinian coral *Pocillopora damicornis* but not its symbiont after acute heat stress. *Front. Mar. Sci.* **7**, 565068 (2020).

62. O. Levy, P. Kaniewska, S. Alon, E. Eisenberg, S. Karako-Lampert, L. K. Bay, R. Reef, M. Rodriguez-Lanetty, D. J. Miller, O. Hoegh-Guldberg, Complex diel cycles of gene expression in coral-algal symbiosis. *Science* **331**, 175 (2011).

63. L. B. Linsmayer, D. D. Deheyn, L. Tomanek, M. Tresguerres, Dynamic regulation of coral energy metabolism throughout the diel cycle. *Sci. Rep.* **10**, 19881 (2020).

64. N. M. Kuntz, D. I. Kline, S. A. Sandin, F. Rohwer, Pathologies and mortality rates caused by organic carbon and nutrient stressors in three Caribbean coral species. *Mar. Ecol. Prog. Ser.* **294**, 173–180 (2005).

65. C. Schlöder, L. D'Croz, Responses of massive and branching coral species to the combined effects of water temperature and nitrate enrichment. *J. Exp. Mar. Biol. Ecol.* **313**, 255–268 (2004).

66. S. A. Wooldridge, T. J. Done, C. R. Thomas, I. I. Gordon, P. A. Marshall, R. N. Jones, Safeguarding coastal coral communities on the central Great Barrier Reef (Australia) against climate change: Realizable local and global actions. *Clim. Change* **112**, 945–961 (2012).

67. P. A. Cleves, C. J. Krediet, E. M. Lehnert, M. Onishi, J. R. Pringle, Insights into coral bleaching under heat stress from analysis of gene expression in a sea anemone model system. *Proc. Natl. Acad. Sci. U.S.A.* **117**, 28906–28917 (2020).

68. L. A. Morris, C. R. Voolstra, K. M. Quigley, D. G. Bourne, L. K. Bay, Nutrient availability and metabolism affect the stability of coral–*symbiodiniaceae* symbioses. *Trends Microbiol.* **27**, 678–689 (2019).

69. J. Wiedenmann, C. D'Angelo, E. G. Smith, A. N. Hunt, F. E. Legiret, A. D. Postle, E. P. Achterberg, Nutrient enrichment can increase the susceptibility of reef corals to bleaching. *Nat. Clim. Chang.* **3**, 160–164 (2013).

70. N. Rädecker, C. Pogoreutz, H. M. Gegner, A. Cárdenas, F. Roth, J. Bougoure, P. Guagliardo, C. Wild, M. Pernice, J. B. Raina, A. Meibom, C. R. Voolstra, Heat stress destabilizes symbiotic nutrient cycling in corals. *Proc. Natl. Acad. Sci. U.S.A.* **118**, e2022653118 (2021).

71. M. E. Barron, A. B. Thies, J. A. Espinoza, K. L. Barott, A. Hamdoun, M. Tresguerres, A vesicular Na+/Ca2+ exchanger in coral calcifying cells. *PLOS ONE* **13**, e0205367 (2018).

72. P. Ganot, E. Tambutté, N. Caminiti-Segonds, G. Toullec, D. Allemand, S. Tambutté, Ubiquitous macropinocytosis in anthozoans. *eLife* **9**, e50022 (2020).

73. K. L. Barott, A. A. Venn, A. B. Thies, S. Tambutté, M. Tresguerres, Regulation of coral calcification by the acid-base sensing enzyme soluble adenylyl cyclase. *Biochem. Biophys. Res. Commun.* **525**, 576–580 (2020).

74. C.-H. Huang, J. Peng, Evolutionary conservation and diversification of Rh family genes and proteins. *Proc. Natl. Acad. Sci.* **102**, 15512–15517 (2005).

75. H. Soreq, S. Seidman, *Xenopus* oocyte microinjection: From gene to protein. *Methods Enzymol.* **207**, 225–265 (1992).

76. C. M. Veauvy, P. J. Walsh, M. D. Mcdonald, Effect of elevated ammonia on tissue nitrogen metabolites in the ureotelic gulf toadfish (*Opsanus beta*) and the ammoniotelic midshipman (*Porichthys notatus*). *Physiol. Biochem. Zool.* **82**, 345–352 (2009).

77. A. J. Kempers, C. J. Kok, Re-examination of the determination of ammonium as the indophenol blue complex using salicylate. *Anal. Chim. Acta* **221**, 147–155 (1989).

78. C. Shinzato, E. Shoguchi, T. Kawashima, M. Hamada, K. Hisata, M. Tanaka, M. Fujie, M. Fujiwara, R. Koyanagi, T. Ikuta, A. Fujiyama, D. J. Miller, N. Satoh, Using the *Acropora digitifera* genome to understand coral responses to environmental change. *Nature* **476**, 320–323 (2011).

79. R. C. Edgar, MUSCLE: A multiple sequence alignment method with reduced time and space complexity. *BMC Bioinformatics* **5**, 113 (2004).

80. A. Stamatakis, RAxML version 8: A tool for phylogenetic analysis and post-analysis of large phylogenies. *Bioinformatics* **30**, 1312–1313 (2014).

81. E. L. Sonnhammer, G. von Heijne, A. Krogh, A hidden Markov model for predicting transmembrane helices in protein sequences. *Proc. Int. Conf. Intell. Syst. Mol. Biol.* **6**, 175–182 (1998).

82. A. Krogh, B. Larsson, G. Von Heijne, E. L. L. Sonnhammer, Predicting transmembrane protein topology with a hidden Markov model: Application to complete genomes. *J. Mol. Biol.* **305**, 567–580 (2001).

83. M. E. Jørgensen, H. H. Nour-Eldin, B. A. Halkier, in *Biotechnology of Plant Secondary Metabolism: Methods and Protocols*, A. G. Fett-Neto, Ed. (Springer Science & Business Media, 2016); http://link.springer.com/10.1007/978-1-4939-3393-8, vol. 1405, pp. 99–107.

84. K. Barott, M. Tresguerres, Immunolocalization of proteins in corals: The V-type H^+-ATPase proton pump. *Bio-protocol* **5**, e1573 (2015).

Trial	Time	# cells with symbiosomal ayRhp1 signal
1	1330	35
1	1730	27
1	1830	22
1	2300	12
1	730	24
1	830	31
2	1330	29
2	1730	18
2	1830	21
2	2300	15
2	730	16
2	830	25
3	1330	28
3	1730	22
3	1830	12
3	2300	12
3	730	29
3	830	28

cells with non-symbiosomal ayRhp1 signal
15
23
28
38
26
19
21
32
29
35
34
25
22
28
38
38
21
22